STUDY OF ELECTRON-ELECTRON (e-e) AND ELECTRON-HOLE (e-h) INTERACTIONS IN GRAPHENE ON SIO_2/SI INTERFACES USING SPECTROSCOPY ELLIPSOMETRY

Tan Ee Cheng (A0072794U)

Supervisor
Assistant Professor Andrivo Rusydi

Co-Supervisor
Dr. Pranjal Gogoi

A Thesis

Presented to the Faculty of Science of the

National University of Singapore

In Partial Fulfillment of the Requirements for the Degree

Bachelor of Science (Honors.) In Physics

2014

ABSTRACT

Graphene is a two-dimensional carbon honeycomb structure that gained popularity due to its excellent electronic properties, such as the ballistic electron transport and outstanding optical and mechanical properties [1]. In this thesis, we study the optical properties of graphene on SiO2/Si using spectroscopic ellipsometry. Our results show that many body effects, in particular the electron-electron (e-e) and electron-hole (e-h) interactions manifest themselves in the graph of optical conductivity of graphene. The strong e-h interactions is observed and it is prominent from the asymmetric resonance peak at 4.65eV. This observed excitonic resonance can be explained by the Fano model, which describes the residing of a discrete excitonic state in the band continuum. Comparing our experimental results with the theoretical calculations of the optical conductivity of a free-standing graphene, we found that the spectrum for graphene on SiO2/Si blue shifted and is less asymmetric. This could be due to an inaccurate optical model used or it could suggest a screening of e-h interactions due to the graphene-SiO2 interaction.

ACKNOWLEDGEMENT

I would like to thank my supervisor Assistant Professor Andrivo Rusydi for providing me with the opportunity to do my honors project in the Singapore Synchrotron Light Source (SSLS). He is greatly appreciated for the guidance, teaching and the continuous support and encouragement provided throughout this period of time. Without him, completing this thesis would be an impossible task.

I would also like to express my gratitude and appreciation to Dr. Pranjal Kumar Gogoi and the researchers and staff in SSLS for their assistance and the advices given to us. We are particularly indebted to Dr Pranjal, without whom this thesis and the data analysis will be an arduous task to complete. He also gave us valuable advices and guidance throughout the year, despite his busy schedule.

I would like to give special thanks to my fellow classmate, Mr. Tay Shengyu for his inputs and encouragement as we worked very closely together for our final year project.

I would like to thank the Ministry of Education (MOE) for providing me with a fully funded opportunity to pursue my B.Sc. (Honors) degree.

Finally, I would like to thank my family members and my girlfriend for their love and support during this entire process.

Contents

LIST OF FIGURES

ORGANISATION OF MATERIALS

In Chapter 1, we give a review of optical physics, giving important equations that will be used in the spectroscopy ellipsometry and curve fitting. Also, a general overview of the band structures and properties of Silicon (Si) and graphene will be given. Then we give a motivation of our thesis to end off the chapter.

In Chapter 2, the experimental technique - spectroscopy ellipsometry will be introduced. In particular, we will be discussing on the equipment components and the quantities it measured. We then discuss about the mathematics behind the ellipsometry and provide a justification on the use of spectroscopy ellipsometry for our experiment through a simulation of another experiment called the reflectance spectroscopy,

In Chapter 3, we discuss about the data analysis of spectroscopy ellipsometry, in particular the curve fitting technique. We will give an evaluation of this technique, and discuss about the strengths and weaknesses.

In Chapter 4, the experimental results will be presented. We will also discuss about our results and the excitonic effects in graphene on SiO2/Si.

In Chapter 5, a summary of our findings will be given. We will also be giving some important future directions, in order to further study graphene on SiO2/Si optical properties in further details.

CHAPTER 1 INTRODUCTION

Recent experiments are carried out in order to understand the properties of the two dimensional Dirac fermions in a graphene layer, due to its excellent electronic properties. The optical properties of graphene are also extensively studied using different experimental set-ups, in particular the spectroscopy ellipsometry is widely used due to the high degree of accuracy [2]. The spectroscopy ellipsometry is a non-destructive and simple experimental technique that measures the change in polarization state in the light, after reflected off the sample [3-4]. This chapter provides review on two components, namely the theoretical background for optical physics as well as the theoretical background to our sample used so as to understand the optical properties of matter as well as the necessary equations used in ellipsometry.

1.1 THEORETICAL BACKGROUND – OPTICAL PHYSICS

1.1.1 STANDARD WAVE PROPAGATION

In 1849, Maxwell have shown that light has the characteristics of waves, with electromagnetic properties that follow the electromagnetic theory. The propagation of an electromagnetic wave can be derived from the well known Maxwell‟s equations below.

$$\nabla . \mathbf{E} = \frac{\rho}{\varepsilon} \tag{1.1}$$

$$\nabla . \mathbf{B} = 0 \tag{1.2}$$

$$\nabla \times \mathbf{E} = -\frac{\partial \mathbf{B}}{\partial t} \tag{1.3}$$

$$\nabla \times \mathbf{B} = \mu\left(\varepsilon\frac{\partial \mathbf{E}}{\partial t} + \mathbf{J}\right) \tag{1.4}$$

Where **E** is the electric field and **B** is the magnetic induction. ε and μ are the permittivity and permeability of the materials. Also, ρ is the charge density and **J** is the current density, such that **J**=ζ**E**, where ζ is the conductivity.

Multiplying both sides of Equation (1.3), we get:

$$\nabla \times \nabla \times \mathbf{E} = -\frac{\partial \nabla \times \mathbf{B}}{\partial \mathrm{t}} \tag{1.5}$$

Using the relation $\nabla \times (\nabla \times \mathbf{E}) = \nabla(\nabla.\mathbf{E}) - \nabla^2\mathbf{E}$, and taking ρ to be zero, Equation (1.5) can then be written as:

$$\nabla^2\mathbf{E} = \mu\varepsilon\frac{\partial^2\mathbf{E}}{\partial \mathrm{t}^2} + \mu\sigma\frac{\partial \mathbf{E}}{\partial \mathrm{t}} \tag{1.6}$$

Equation (1.6) is the wave equation of an electromagnetic wave inside a conductor. When we consider electromagnetic wave propagation in vacuum, the permittivity ε will be written as ε_0 while the permeability μ is written as μ_0. Putting the conductivity ζ as zero, we can rewrite Equation (1.6) as:

$$\nabla^2\mathbf{E} = \varepsilon_o\mu_o\frac{\partial^2\mathbf{E}}{\partial \mathrm{t}^2} \tag{1.7}$$

Comparing with the wave equation of a general wave which has the form $\nabla^2\mathbf{f} = \frac{1}{\mathrm{s}^2}\frac{\partial^2\mathbf{f}}{\partial \mathrm{t}^2}$ where s is the speed of the wave, the speed of light in vacuum can be obtained to be:

$$c = \frac{1}{\sqrt{\mu_o\varepsilon_o}} = 2.99792 \times 10^8 m/s \tag{1.8}$$

Equation (1.7) has the solution expressed by:

$$\mathbf{E} = \mathbf{E}_o \exp[\mathrm{i}(\omega \mathrm{t} - \kappa \mathrm{x})] \tag{1.9}$$

such that κ is the propagation number given by 2π/λ and $\mathbf{E}_o$ is the amplitude of the wave. The same procedure can be carried out on the B field, and it has the same form as Equation (1.9) giving:

$$\mathbf{B} = \mathbf{B}_o \exp[i(\omega t - \kappa x)] \tag{1.10}$$

The direction of light propagation is perpendicular to **E** and **B**, and there is a relation given by:

$$\mathbf{E} = c\mathbf{B} \tag{1.11}$$

1.1.2 PROPAGATION OF LIGHT IN SOLIDS

When light propagates into an optically different medium, the refraction of light takes place. The refraction of light depends on the refractive index, n and n is defined to be:

$$n = \frac{c}{s} \tag{1.12}$$

whereby s is the speed of light in the medium. From Equation (1.12), light waves travel slower in a medium with high n. In the case when there is no light absorption in the media, the propagation number, κ can be written in terms of the refractive index, n as follows:

$$\kappa = \frac{2\pi n}{\lambda} = \frac{\omega n}{c} \tag{1.13}$$

Equation (1.13) is the propagation number of light waves in a transparent medium. If Equation (1.13) is plugged into Equation (1.9), it follows that:

$$\mathbf{E} = \mathbf{E}_o \exp[i(\omega t - 2\pi n x/\lambda)] \tag{1.14}$$

Equation (1.14) illustrates the waveform when the light waves travelling in a transparent medium. One can see from this equation that the wavelength of light becomes λ/n, simply by comparing with Equation (1.9). One notable characteristic of this equation is that the amplitude of the wave will remain constant as it propagates in the medium.

In the event when light travels in an absorbing medium, Equation (1.13) must be modified to include the extinction coefficient k, a quantity used to describe light absorption in a media. A complex refractive index N is defined, such that

$$\mathrm{N} = \mathrm{n} - \mathrm{ik} \tag{1.15}$$

and the n in Equation (1.13) must be replaced with N, to describe light propagation in an absorbing medium. To show how the amplitude changes of the waveform changes when light propagates in an absorbing medium, one can substitute Equation (1.13) into Equation (1.9) again. It follows that:

$$\begin{aligned} \mathbf{E} &= \mathbf{E}_0 \exp\left[\mathrm{i}\left(\omega \mathrm{t} - \frac{2\pi \mathrm{Nx}}{\lambda}\right)\right] \\ &= \mathbf{E}_0 \exp\left(-\frac{2\pi \mathrm{kx}}{\lambda}\right) \exp\left[\mathrm{i}\left(\omega \mathrm{t} - \frac{2\pi \mathrm{nx}}{\lambda}\right)\right] \end{aligned} \tag{1.16}$$

Equation (1.16) shows an exponential drop in the amplitude of the wave as it propagates into the medium. Meanwhile, the change in the wavelength of light remains at λ/n. This leads to an important conclusion: the absorption of light has no effects on the wavelength.

There is an important point to be mentioned. In this thesis, the refractive index N is defined as N=n-ik as shown in Equation (1.15) and the phase of the wave is expressed to be (ωt-κx). Some literatures might define N=n+ik, and in this case, the phase of the wave must be expressed in (-ωt+κx), so that the decay of the electromagnetic wave in the medium can be expressed in exp(-2πkx/λ).

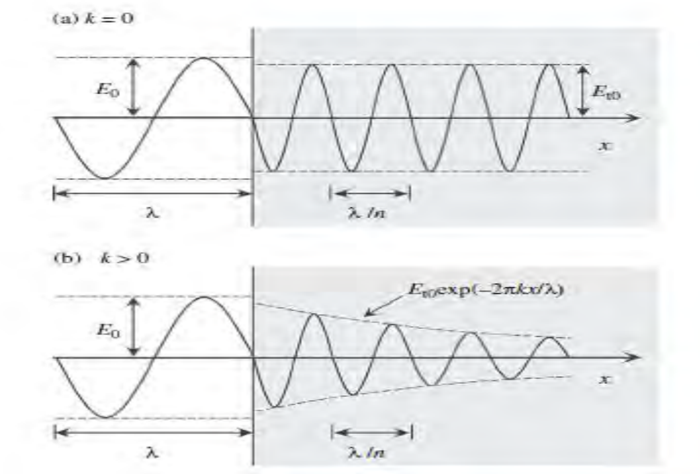

Figure 1.1 - The propagation of light waves in (a) a transparent medium and (b) an absorbing medium. From [3].

1.1.3 BEER'S LAW

Using Equation (1.16), one can find the intensity of light propagating in the medium using the following relation:

$$\mathrm{I} = |\mathbf{E}|^2 = \mathbf{E}^*\mathbf{E} \tag{1.17}$$

$$\mathrm{I} = |\mathbf{E_0}\exp(-2\pi \mathrm{kx}/\lambda)\,|^2 = |\mathbf{E}_{\mathbf{0}}|^2\exp\left(-\frac{4\pi \mathrm{kx}}{\lambda}\right) \tag{1.18}$$

Equation (1.16) shows that the intensity of light decreases exponentially in the medium. This is often referred to as the Beer‟s Law, an empirical relation:

$$\mathrm{I} = \mathrm{I_o}\exp(-\alpha \mathrm{d}) \tag{1.19}$$

where α is the absorption coefficient of the medium and d is the distance from the surface. If Equation (1.18)and (1.19) is compared, then

$$\alpha = \frac{4\pi \mathrm{k}}{\lambda} \tag{1.20}$$

Equation (1.20) shows that the absorption coefficient is related to the extinction coefficient,k.

1.1.4 DIELECTRIC CONSTANTS

From the previous section, it has been shown that the propagation of light in a medium is largely described by the complex refractive index, N. In this section, it will be shown that N is actually determined by the dielectric polarization generated, when external E field impinges on the medium.

In dielectrics, electric charges are not able to move freely as atoms are bound very strongly together. Nonetheless, under the application of the external E field, there will still be a modification of the positive and negative charges as they react differently to the E field. Due to this modification, there is a spatial distribution of the positive and negative charges, such that there will be regions that are more electrically positive and negative. This is further illustrated in Figure 1.2.

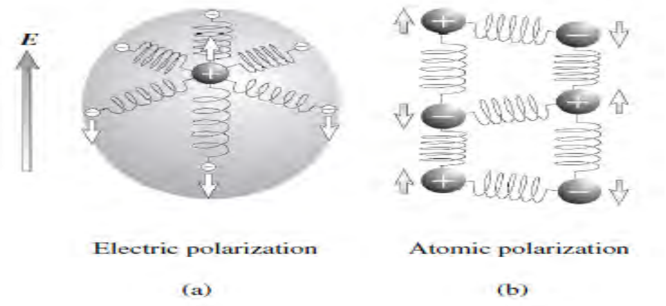

Figure 1.2 - Dielectric polarization of a dielectric under external electric field. a) The electric polarization b) The atomic polarization. From [3].

Figure 1.2a shows the electric polarization. Under the influence of the electric field, the positions of the negatively charged electron as well as the positively charged charges in the atom will be distorted in opposite directions. For ionic crystals like NaCl, which consists of positive and negative charged ions, atomic or ionic polarization takes place.

The extent of polarization, **P** in a material is determined by dielectric constant or the permittivity ε_p . More often, the relative permittivity or the relative dielectric constant is used, and it has the form of:

$$\varepsilon = \frac{\varepsilon_p}{\varepsilon_o} \qquad (1.21)$$

where ε_o is the permittivity in vacuum.

The refractive index, N defined in the previous section is related to the relative dielectric constant as below:

$$N^2 = \varepsilon \qquad (1.22)$$

ε is a complex number and the complex dielectric constant is defined as:

$$\varepsilon = \varepsilon_1 - i\varepsilon_2 \qquad (1.23)$$

If we combine Equation (1.15) and (1.23), we can find that

$$\varepsilon_1 = n^2 - k^2 \qquad (1.24)$$

$$\varepsilon_2 = 2nk \qquad (1.25)$$

and

$$n=\{[\varepsilon_1 + (\varepsilon_1^2 + \varepsilon_2^2)^{1/2}] /2\} \qquad (1.26)$$

$$k=\{[-\varepsilon_1 + (\varepsilon_1^2 + \varepsilon_2^2)^{1/2}] /2\} \qquad (1.27)$$

From Equation (1.22), one can see that the easier electric dipole is formed (higher ε), the slower the light propagation in the solid is.

ε has been treated as a single complex number so far, but in actual experiments, it will change according to the angular frequency ω of incident light applied to the solid. One can see this from Figure (1.3), a graph of dielectric function versus energy of Aluminum metal.

In our experiment, the graph of dielectric function versus energy of graphene on SiO2/Si will be plotted in order to study the optical properties.

1.1.5 DRUDE AND LORENTZ MODEL

There are many dielectric models that describe the motions of electrons under the application of electric field, in particular, we use the Drude - Lorentz dielectric model for our curve fitting of experimental results. The Lorentz oscillator model is applicable to insulators and semiconductors while the Drude model is applicable to metals, with free electron carriers.

(a) LORENTZ MODEL

In a classical picture, the electrons can be modeled to be connected to the positively charged atomic nucleus with a spring. Once the light is impinged onto the sample, the electric field with $E=E_0 \exp(i\omega t)$ will induce an electric polarization mentioned in the previous section. Using Newton"s second law, one can describe the motion of the electron like an oscillator.

$$m\frac{d^2x}{dt^2} = -m\gamma\frac{dx}{dt} - m{\omega_o}^2 x - eE_o \exp(i\omega t) \qquad (1.28)$$

such that the first term on the right represents the viscous force, and ϒ is the damping coefficient (electron motion damped by phonons), ω_o is the resonant frequency of the oscillator, while the second term refers to the restoring force on electrons and the third term represents the applied field.

Equation (1.28) gives an solution of x(t)=*b* exp (iωt), such that b has the form of

$$b = \frac{-eE_o}{m}\frac{1}{({\omega_o}^2 - \omega^2) + i\gamma\omega} \qquad (1.29)$$

Considering a solid with N_e number of electrons per unit volume, the dielectric polarization P is expressed as $P= -eN_e b\exp(i\omega t)$. Meanwhile, P is also related to the dielectric constant with the following equation:

$$\varepsilon = \varepsilon_\infty + \frac{P}{\varepsilon_o E} \qquad (1.30)$$

Combining Equation (1.29) and Equation (1.30), the dielectric function is expressed to be:

$$\varepsilon = \varepsilon_\infty + \frac{e^2 N_e}{\varepsilon_o m}\frac{1}{({\omega_o}^2 - \omega^2) + i\gamma\omega} \qquad (1.31)$$

The above described is only applicable to 1 oscillator. When there are many oscillators, Equation (1.31) will become:

$$\varepsilon = \varepsilon_\infty + \sum_{\mathrm{i}} \frac{{\omega_{\mathrm{pi}}}^2}{({\omega_{\mathrm{oi}}}^2 - \omega^2) + \mathrm{i}\gamma_{\mathrm{i}}\omega} \tag{1.32}$$

such that ω_p is the plasma frequency, given by $e^2N_e/\varepsilon_o m$, and i refers to the i^{th} oscillator. Equation (1.32) also shows that the dielectric ε is a function of the frequency of light.

(b) DRUDE MODEL

As mentioned above, the Drude model can be used to model the dielectric functions of metals or semiconductors with free carriers. The dielectric function can be gotten from Equation (1.31) by putting ω_0, the resonant frequency to be 0, since the carriers are free to move and they are not under the effect of a restoring force that gives rise to resonant frequency. If we assume that the free carriers are also subjected to the same damping force, Υ, then we can get:

$$\varepsilon = \varepsilon_\infty + \frac{\omega_{\mathrm{p,D}}^2}{(-\omega^2) + \mathrm{i}\gamma\omega} \tag{1.33}$$

such that $\omega_{\mathrm{p,D}}^2$ is the plasma frequency, where $\omega_{\mathrm{p,D}}^2 = e^2N_{e,f}/\varepsilon_o m_e$ and $N_{e,f}$ is the concentration of the free electrons. The Drude model described predicts a frequency dependent free carrier conductivity to be:

$$\sigma(\omega) = \frac{\sigma_0}{1 + \mathrm{i}\omega\tau} = \sigma_1 - \mathrm{i}\sigma_2 \tag{1.34}$$

where ζ_0 and τ are the DC conductivity and the scattering time of the electrons respectively, while ω represents the frequency of light. It turns out that [5]:

$$\sigma_0 = \frac{n_e e^2 \tau}{m_e} \quad , \Upsilon = \frac{1}{\tau} \tag{1.35}$$

It is also notable that the optical absorbance at normal reflectivity is related to the optical sheet conductivity by:

$$A(\omega) = \frac{4\pi}{c}[\sigma_1(\omega)] \tag{1.36}$$

Thus, looking at the absorbance curve can already give us information of the optical conductivity.

Figure 1.3 below shows dielectric curve of an Aluminum metal measured from spectroscopy ellipsometry.

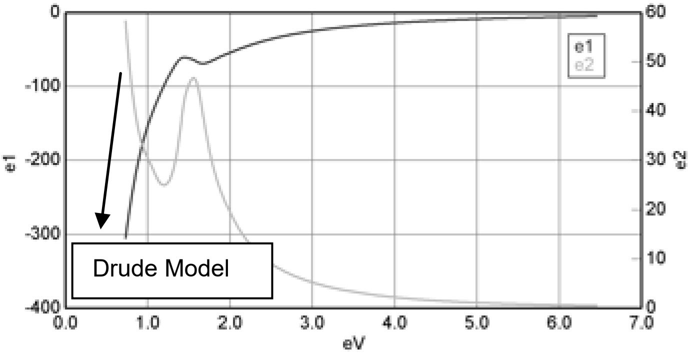

Figure 1.3 - Dielectric Functions of Aluminum. From [6].

The Drude model is normally dominant at low energy of light. The peak of ε_2 at around 1.6eV shown in Figure 1.3 represents the absorption of light, such that the corresponding frequency represents the resonant frequency of the oscillator predicted by the Drude-Lorentz model. Looking at Equation (1.25) one can see that the ε_2 is proportional to k, the extinction coefficient. Hence, looking at the peaks in curve of ε_2 tells us the frequency of light that has been absorbed significantly, which is related to electrons transition from the valence band to conduction band.

1.1.6 KRAMERS KRONIG RELATION

As mentioned, ε=ε(ω) and due to causality principle, the real part and imaginary parts of ε are not independent. Instead, they are coupled with the Kramers-Kronig relation [7-8]. This gives:

$$\varepsilon_1 - 1 = \frac{2}{\pi} \mathrm{P} \int_0^{\infty} \frac{x\varepsilon_2(x)}{x^2 - \omega^2} dx \qquad (1.37)$$

$$\varepsilon_2 = -\frac{2\omega}{\pi} \mathrm{P} \int_0^{\infty} \frac{\varepsilon_1(x)}{x^2 - \omega^2} dx \qquad (1.38)$$

where the P refers to the principal value integral, such that a singularity will occur when x=ω. The n and k defined in Section 1.12 are also connected with the Kramers-Kronig relation. In Chapter 2 where the comparison of ellipsometry and reflectance spectroscopy is made, the Kramers-Kronig relation will be revisited.

1.1.7 P AND S POLARIZED LIGHT

It is important to review on the theory of P and S polarized light as spectroscopy ellipsometry measures the amplitude as well as the phase difference between the P and S polarized light after reflecting off the surface.

Light can be classified into P and S polarization, such that P- polarized light oscillates parallel to the plane of incidence, while the S- polarized light oscillates in a perpendicular direction to the plane of incidence. It is further illustrated in Figure 1.4 that after light reflection, the P polarized incident and P polarized reflected are in the same plane with the plane of incidence.

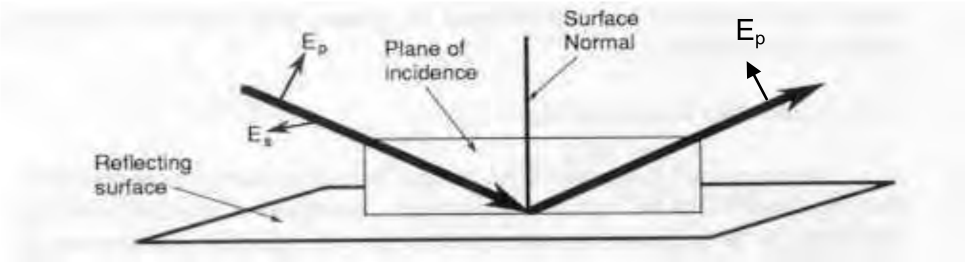

Figure 1.4 - The P- and S polarized light. From [3].

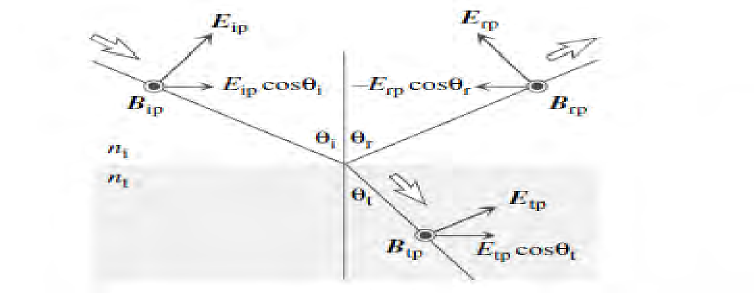

(a) p-polarization

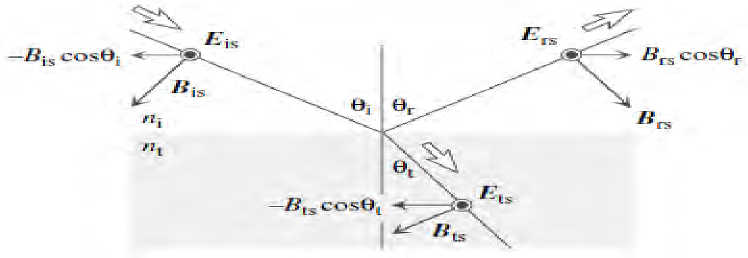

(b) s-polarization

Figure 1.5 - a) The P polarized light, b) The S polarized light. From [3].

1.1.8 FRESNEL'S EQUATION

Figure 1.5a further illustrates the idea of P and S polarization of light. In the figure, Θ_i , Θ_r , and Θ_t represents the incident angle, reflection angle and transmission angle of light respectively. E_{ip}, E_{rp}, E_{tp} represents the amplitude of E field of incident, reflected and transmitted P polarized light while the subscript s represents the S- polarized light. The boundary conditions for E and B require

i) for the p-polarized light to be:

$$E_{ip}\cos\Theta_i - E_{rp}\cos\Theta_r = E_{tp}\cos\Theta_t \quad (1.39)$$

$$B_{ip}+B_{rp}=B_{tp} \tag{1.40}$$

ii) for the s-polarized light to be:

$$-B_{is}\cos\Theta_i + B_{rs}\cos\Theta_r = -B_{ts}\cos\Theta_t \tag{1.41}$$

$$E_{is}+E_{rs}=E_{ts} \tag{1.42}$$

For a medium with a refractive index of N, E=sB from Equation (1.12), such that s is the speed of light in the medium. Using this relation and Equation (1.11), Equation (1.40) can be re-written as:

$$N_i(E_{ip} + E_{rp}) = N_t E_{tp} \tag{1.43}$$

If compare Equation(1.39) and (1.43) and eliminate E_{tp}, one can get the amplitude reflection coefficient of the p polarized light by defining $r_p=E_{rp}/E_{ip}$. Hence,

$$r_p = \frac{E_{rp}}{E_{ip}} = \frac{N_t\cos\theta_i - N_i\cos\theta_t}{N_t\cos\theta_i + N_i\cos\theta_t} \tag{1.44}$$

If the same procedure is carried out for the s-polarized light, the amplitude reflection coefficient of the s polarized light is:

$$r_s = \frac{E_{rs}}{E_{is}} = \frac{N_i\cos\theta_i - N_t\cos\theta_t}{N_i\cos\theta_i + N_t\cos\theta_t} \tag{1.45}$$

r_p and r_s are called the Fresnel equations and they are complex functions, since related to the complex refractive index N. We can hence express r_p and r_s in the polar coordinate representation, such that:

$$r_{p=|r_p|}\exp(i\delta_{r_P}) \tag{1.46}$$

$$r_{p=|r_p|}\exp(i\delta_{r_s}) \tag{1.47}$$

In ellipsometry, the difference between the two phases δ_{r_p} and δ_{r_s} will be measured, and will be further elaborated in Chapter 2.

From the Fresnel‟s equation, we can also find the reflectance, the ratio of reflected intensity and incident intensity to be:

$$R_p = \frac{I_{rp}}{I_{ip}} = |\frac{E_{rp}}{E_{ip}}|^2 = |r_p|^2 \tag{1.48}$$

$$R_s = \frac{I_{rs}}{I_{is}} = |\frac{E_{rs}}{E_{is}}|^2 = |r_s|^2 \tag{1.49}$$

1.1.9 OPTICAL INTERFERENCE IN THIN FILMS

It is important to also review on the optical interference in thin films, in particular the Fresnel‟s equations for a multilayer system. We used optical model of 0123 system (Figure 1.6); 0 is the always defined as the medium air, 1 is medium graphene, 2 is medium SiO2, and lastly 3 is medium Si to describe our sample. This optical model assumes that graphene is smooth and there are no interface layer in between the interfaces. We will be talking more of the optical model in Chapter 4 when we discuss the experimental results, as the optical model is crucial for a good fitting.

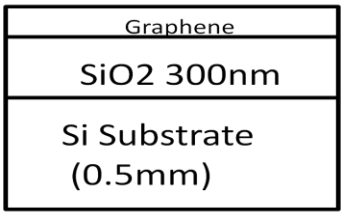

Figure 1.6 - Optical model of sample used in experiment.

The Fresnel‟s equation for a 012 system can be used to evaluate the Fresnel‟s equation for a 0123 system.

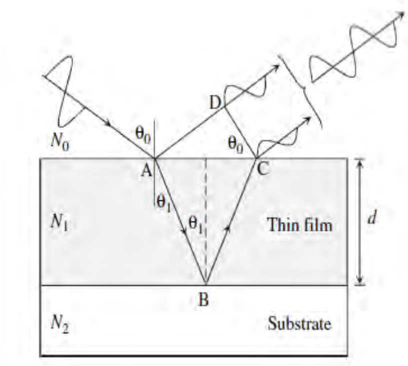

Figure 1.7- Optical model 012 system. From [3].

When an incident light wave is impinged and reflected from the surface of medium 1, shown in Figure 1.7, it will interfere with the light that is reflected off the medium 2. There is a possibility for a constructive interference or a destructive interference, depending on the wavelength of light and the optical constants of the system. Light wave reflected off the medium 1 will be called primary beam, while the wave reflected off the substrate and transmitted out from the thin film will be called the secondary beam.

The phase difference between two beams of light can be found to be:

$$\beta = \frac{2\pi d N_1}{\lambda}\left(\frac{1-\sin^2\theta_1}{\cos\theta_1}\right) = \frac{2\pi d N_1}{\lambda}\cos\theta_1 \qquad (1.50)$$

The Fresnel"s equation for a 012 system for both P- and S- polarized light are expressed as:

$$\begin{aligned} r_{012,p} &= \frac{r_{01,p} + r_{12,p}\exp(-i2\beta)}{1 + r_{01,p} r_{12,p}\exp(-i2\beta)}, \\ r_{012,s} &= \frac{r_{01,s} + r_{12,s}\exp(-i2\beta)}{1 + r_{01,s} r_{12,s}\exp(-i2\beta)} \end{aligned} \qquad (1.51)$$

Equation (1.51) can now be used to find the Fresnel"s equation for a 0123 optical model system in Figure 1.6. For a 123 system, the Fresnel"s equation is:

$$\begin{aligned} r_{123,p} &= \frac{r_{12,p} + r_{23,p}\exp(-i2\beta_2)}{1 + r_{12,p} r_{23,p}\exp(-i2\beta_2)}, \\ r_{123,s} &= \frac{r_{12,s} + r_{23,s}\exp(-i2\beta_2)}{1 + r_{12,s} r_{23,s}\exp(-i2\beta_2)} \end{aligned} \qquad (1.52)$$

such that β_2 is $\frac{2\pi d_2 N_2}{\lambda}\cos\theta_2$ with Θ_1 and Θ_2 as the transmission angles of light in medium 1 and medium 2. The whole of 0123 system has the following Fresnel‟s equation:

$$r_{0123,p} = \frac{r_{01,p} + r_{123,p}\exp(-i2\beta_1)}{1 + r_{01,p}r_{123,p}\exp(-i2\beta_1)}$$
$$r_{0123,s} = \frac{r_{01,s} + r_{123,s}\exp(-i2\beta_1)}{1 + r_{01,s}r_{123,s}\exp(-i2\beta_1)} \qquad (1.53)$$

Combining Equation (1.52) and (1.53), we will get the full form of the Fresnel‟s equation of a 0123 system to be:

$$r_{0123} = \frac{r_{01} + r_{12}\exp(-i2\beta_1) + [r_{01}r_{12} + \exp(-i2\beta_1)]r_{23}\exp(-i2\beta_2)}{1 + r_{01}r_{12}\exp(-i2\beta_1) + [r_{12} + r_{01}\exp(-i2\beta_1)]r_{23}\exp(-i2\beta_2)} \qquad (1.54)$$

We shall see in Chapter 2 the importance of understanding the Fresnel‟s equations, as they are crucial in understanding the ellipsometry.

1.2 THEORETICAL BACKGROUND – PROPERTIES OF SAMPLES

In this section, we give a brief introduction to the „generic" excitons and we will see that these excitons will not be present in graphene. We also give a brief review on the properties on our sample, namely the Si, SiO2 as well as graphene. This is crucial as we study the optical properties of graphene on SiO2/Si.

1.2.1 E-H INTERACTION

e-h interaction refers to the formation of an excitons, such that an electron and hole are bound together by their Coulomb interactions. When a photon excites an electron, a hole is left behind in the valence band, such that the negatively charged electron is attracted to the positively charged hole .

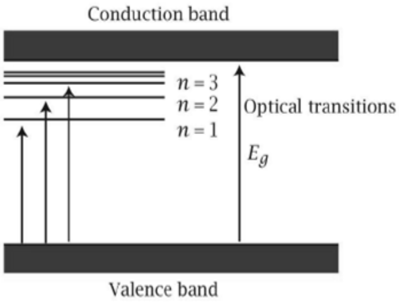

Figure 1.8 – The excitons energy levels. From [9].

One can see from Figure 1.8 that the energy of the excitons are also quantized, with n=1 below the conduction band. The binding energy of the excitons is :

$$E_{Bind} = \frac{R_x}{n^2} \tag{1.55}$$

such that R_x refers to the Rydberg formula of the hydrogen atom, giving:

$$R_x = \frac{1}{2}\left[\frac{m_e q^4}{(4\pi\varepsilon_0)^2\hbar^2}\right]\left(\frac{\mu}{\epsilon^2 m_e}\right) \tag{1.56}$$

such that μ is the effective mass of the system, where

$$\frac{1}{\mu} = \frac{1}{m_e} + \frac{1}{m_h} \tag{1.57}$$

There are two generic types of excitons, the Wannier Mott type excitons and the Frenkel excitons. Figure 1.9 below illustrates these two excitons.

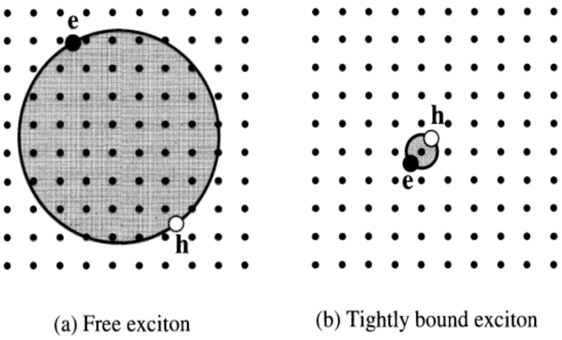

Figure 1.9 – a) The Wannier Mott excitons. b) The Frenkel excitons. From [5].

The Wannier-Mott excitons have a larger radius that encompasses many atoms while the Frenkel excitons has smaller radius. The radius of an exciton can be quantified to be:

$$a_x = \frac{4\pi\varepsilon\varepsilon_0\hbar^2}{\mu q^2} \qquad (1.58)$$

With Equation (1.55) and (1.58), one can that the binding energy of an excitons drops when the radius of the excitons are bigger. Thus, Wannier Mott excitons have weaker binding energy than the Frenkel excitons.

A stable excitons will be formed if the binding energy is strong enough to protect itself from the collision of phonons. Since the energy of phonons is proportional to the temperature by $\sim k_BT$, where k_B is the Boltzmann"s constant, an excitons can only be observed when E_{Bind} is greater than k_BT. Typically, a Wannier-Mott excitons has a binding energy at around 0.01 eV, which corresponds to a very low temperature. Meanwhile, Frenkel excitons, with high binding energy can be observed at a room temperature, with a larger binding energy of 0.1-1eV. We shall see that these types of excitons are not the ones that influenced the optical conductivity of graphene as graphene has zero band gap. Instead, a new type of excitons, called the resonant excitons will be reported from our experimental results.

1.2.2 PROPERTIES OF c-SI AND SIO$_2$

Si is a group IV semiconductor that has a face-centered cubic (FCC) lattice with a two atom basis, and it has a diamond structure shown below in Figure 1.10.

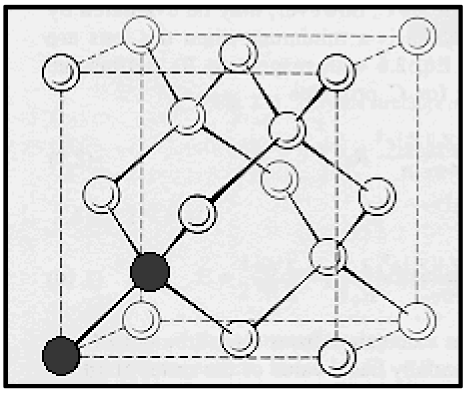

Figure 1.10 – Si crystal structure. From : www.princton.edu.

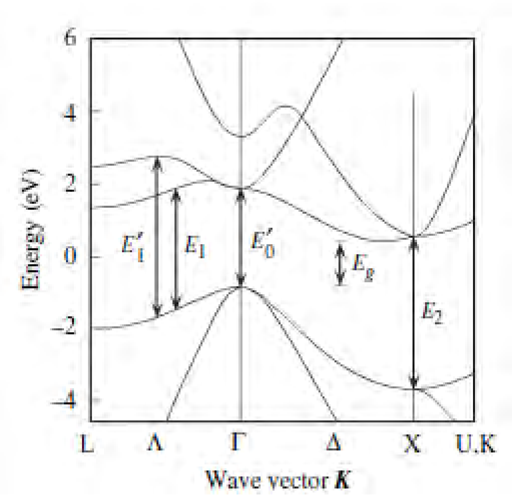

Figure 1.11 – Electronic band structure of Si. From [10].

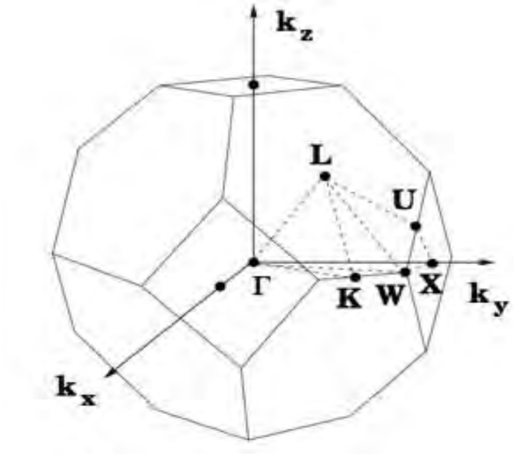

Figure 1.12 – Cubic crystal of Si. From: http://www.cmmp.ucl.ac.uk/.

Figure 1.11 shows the theoretical electronic band structure, calculated using the local-density functional theory (LMTO) method.[10] One can see clearly in the band structure above that Si is a indirect band gap semi conductor, where the band gap is labeled as E_g . In momentum space where k=0(Γ point) lies the maximum of the valence band, while the minimum of the conduction band is at region X. This indirect band gap is found to be 1.12eV theoretically from [10]. Also, two bands converge at the valence band maximum at the Γ point (degenerate bands), and these bands are called the heavy and light hole bands; with the flatter one being heavy hole band and steeper one being light hole band, since the effect mass, m^* is proportional to $(\frac{d^2E}{dk^2})^{-1}$. Due to the different masses, the light holes will react faster than the heavy holes in the presence of electric field. Also, the density of state of the conduction (g_c) and valence band (g_v) near band edge (assuming a parabolic shape) are:

$$g_{\,c} = \mathrm{C}\,\mathrm{m}_c^{*\frac{3}{2}}(\mathrm{E} - \mathrm{E_C})^{1/2} \tag{1.59}$$

$$g_v = \mathrm{C}\,\mathrm{m}_{hh}^{*\,\frac{3}{2}}(\mathrm{E_v} - \mathrm{E})^{1/2} \tag{1.60}$$

such that C=$\left(\frac{1}{2\pi^2}\right)(\frac{2}{h^2})^{3/2}$.

Thus, the above equations suggests that there is a higher density of states of heavy holes.

The substrate used in our experiment is crystalline c-Si whereby the crystal resembles an ordered arrangement and the figure below shows the dielectric function of c-Si studied with spectroscopic ellipsometry [11].

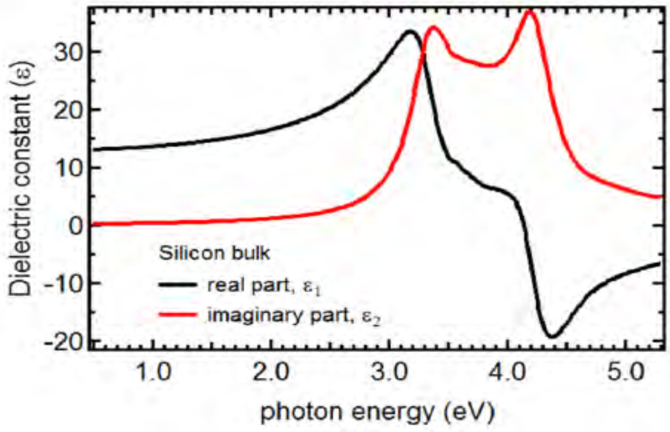

Figure 1.13 – Dielectric function of c- Si. From [11].

There are two absorption peaks in ε_2 spectrum, one at 3.4eV which corresponds to optical transition of $E_o^{\backslash}$ and E_1 shown in Figure 1.11 while another at 4.25eV which corresponds to the optical transition of E_2. Many dielectric spectrum of c-Si can be found here [3,12-13].

Meanwhile, SiO2 is known to be insulating and it is transparent in our experiment energy limit, with a large band gap of 8.9eV [14]. It must be noted that natural oxidation process will occur to the Si samples, such that a thin layer of native oxide is formed on the surface of Si.

1.2.3 PROPERTIES OF GRAPHENE

Graphene was quickly acknowledged as an interesting material due to its unique band structures and excellent electronic properties. Graphene is a two-dimensional (2D) sheet of honeycomb structure made from hexagonal arrangements of carbon atoms as shown in figure below.

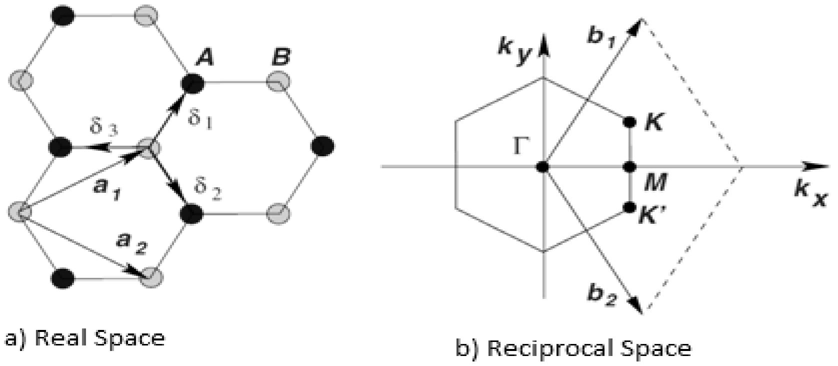

a) Real Space

b) Reciprocal Space

Figure 1.14 – a) The lattice structure of graphene. b) The corresponding Brillouin zone. From [15].

The Bravais lattice are chosen such that the vectors $\mathbf{a_1}$, $\mathbf{a_2}$ are represented by:

$$\mathbf{a_1} = \frac{a}{2}(3, \sqrt{3}), \mathbf{a_2} = \frac{a}{2}\ (3, -\sqrt{3}) \qquad (1.61)$$

and the corresponding reciprocal space has the reciprocal lattice vector represented as:

$$\mathbf{b_1} = \frac{2\pi}{3a}(1, \sqrt{3}), \mathbf{b_2} = \frac{2\pi}{3a}(1, -\sqrt{3}) \qquad (1.62)$$

and the hexagon drawn in Figure 1.14b is the first Brillouin zone (FBZ). The κ and $\kappa^{|}$ represents the corners of the FBZ and they have the coordinates of:

$$\boldsymbol{\kappa} = \left(\frac{2\pi}{3a}, \frac{2\pi}{3a\sqrt{3}}\right), \boldsymbol{\kappa}^{|} = \left(\frac{2\pi}{3a}, -\frac{2\pi}{3a\sqrt{3}}\right) \qquad (1.63)$$

Also, the nearest neighbor in real space shown in Figure 1.14a is represented by:

$$\boldsymbol{\delta_1} = \frac{a}{2}(1, \sqrt{3}), \boldsymbol{\delta_2} = \frac{a}{2}(1, -\sqrt{3}), \boldsymbol{\delta_3} = -a(1,0) \qquad (1.64)$$

Graphene has the band structure shown [16].

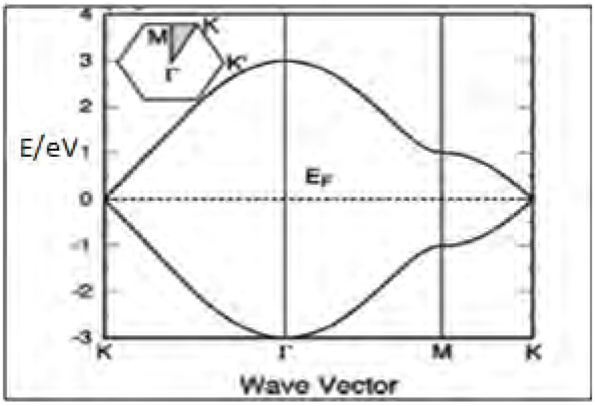

Figure 1.15 – Band structure of graphene. From [16].

We see that at the points κ and κ', the linear valence band and the conduction bands meet. The π and π^* states of carbon atoms form this valence and conduction bands respectively, and because they touch at the point κ at the Dirac point, graphene has zero band gap.

Near the points κ and κ', the energy band is represented by a linear energy dispersion, which directly implies that electrons in graphene have zero effective mass and they move at a speed 300 times smaller than the speed of light[1,16].

Also, from Figure 1.15, the point M represents a saddle point in the energy spectrum. This saddle point is known as the van-Hove singularity. The M point contributes an optical conductivity at around 5.2eV, but reduces to around 4.6eV due to e-h interactions [17]. This will be elaborated in the next sub-section

Graphene exhibits excellent electronic transport properties. Electrons in graphene exhibits ballistic transport, and it moves with a Fermi velocity of v_F~10^6 ms^{-1}. This makes graphene a new candidate for making transistors [16,18]. However, for graphene on SiO_2/Si, it was found that the mobility of carriers dropped from 200000cm^2 V^{-1}s^{-1} to only a few thousands or tens of thousands cm^{2}V^{-1}s^{-1} due to scattering induced by the substrate [16]. Thus, in order to reap the excellent electronic properties of graphene, graphene were made suspended so that there is minimum interaction of graphene with the substrates [18]. The electronic properties of graphene are in general extensively studied.

(a) OPTICAL PROPERTIES OF GRAPHENE

The optical conductivity of graphene shows characteristics of intraband and interband transitions, at different energy range [17].

Optical absorption in graphene is dominated by intraband transitions (free carriers) at low photon energies in the far-infrared range. Since the speed of light c is much higher than that the Fermi velocity of Dirac fermions, such that the c/v_F ~ 300, momentum will not be conserved when an electron absorbs light by an intraband optical transition. In order to conserve momentum, it requires the need of extra scattering with phonons or defects. From Figure 1.16 below, one can see a simple illustration of the intraband optical transition.

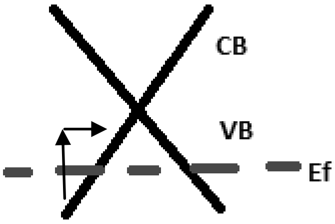

Figure 1.16 – The intraband optical transition.

Recent study of hole and electron doped CVD graphene at room temperature [19] using far-infrared spectroscopy shows that the corresponding $\zeta_1(\omega)$ curves can be fitted by using the Drude model, which directly shows that in the far-infrared energy range, the absorption is dominated by free carrier.

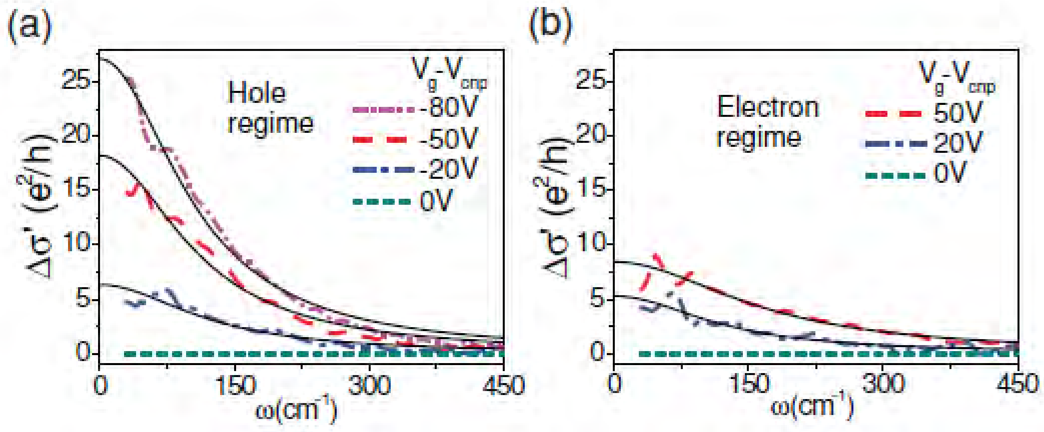

Figure 1.17 – a) Change in ζ_1 of a hole-doped graphene due to doping. b) change in ζ_1 of a electron-doped graphene due to doping. From [19].

Meanwhile, at above far-infrared region, interband transitions from the valence band to the conduction band take place and it has been found that there is a frequency independent universal absorption or ζ_1. Calculated in [20], the ζ_1 of graphene at zero temperature is found to be proportional to $\frac{\pi e^2}{2h}$. The transmission of light was also calculated to be T= 1-πα~0.977, where α refers to the fine structure constant, $\frac{e^2}{\hbar c}$. This theoretical calculation is supported by the experimental work described in [21]. Using a reflectance spectroscopy measurement, Mak.et.al found that the absorbance at infrared to visible energy range is frequency independent and most importantly, close to πα=0.023. This is shown in diagram below.

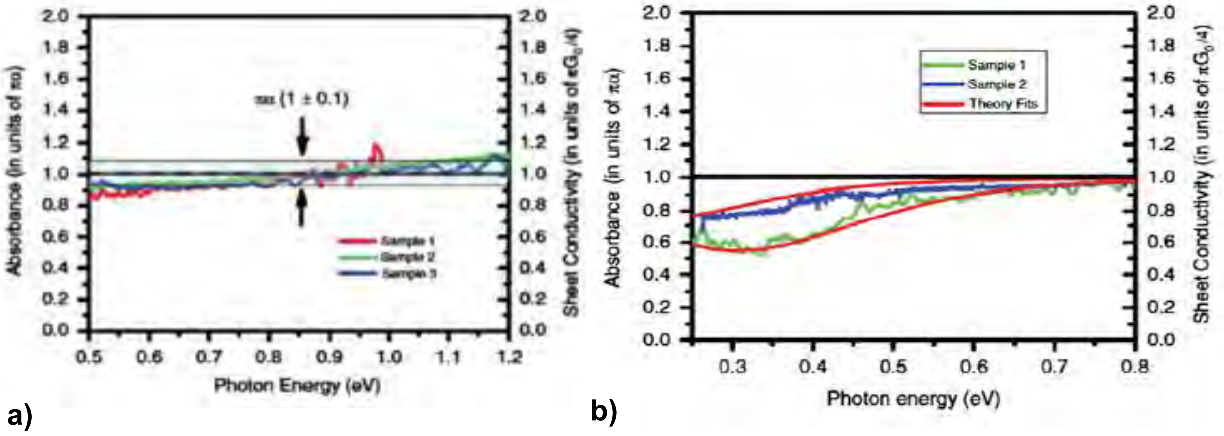

Figure 1.18 – a) Absorbance of 3 different graphene samples using reflectance spectroscopy from 0.5eV to 1.2eV. b) Absorbance of graphene samples from 0.25eV to 0.8eV. From [21].

Reference [21] did not specify the differences between each of the samples used in the experiment for the absorbance. Nonetheless, we can see that the general trend of the absorbance of graphene in that particular energy range. However, if one look closely at Figure 1.18b, there is a slight departure from the universal absorbance at lower energy.

The slight departure is mainly due to the effect of finite temperature when the experiment was conducted and unintentional doping due to the preparation of sample. As a result, the calculation of optical conductivity due to interband transition takes the form of [21]:

$$\sigma(\omega, \mathrm{T}) = \frac{\pi e^2}{4h}\left[\tanh\left(\frac{\hbar\omega + 2\mu}{4k_B T}\right) + \tanh\left(\frac{\hbar\omega - 2\mu}{4k_B T}\right)\right] \tag{1.65}$$

where μ refers to the chemical potential from the Dirac point. The shift of chemical potential is due to the doping.

From the above equation, it can be calculated that only when the photon energy, $\hbar\omega >> 2\mu$ and $\hbar\omega >> k_B T$, the optical conductivity will assume the universal conductivity value. It should be noted that interband transition will not take place at energy $\hbar\omega < 2\mu$. This is due to the Pauli-blocking of transition states caused by the doping. In this case, intraband transition is dominant.

Lastly, we shall discuss the absorbance spectrum of graphene in the UV region and beyond. Theoretical studies of the absorbance of graphene using the GW calculations, which takes into considerations of the band to band and Coulomb e-e interactions is shown as dotted curve below. Meanwhile, when the attractive e-h interaction is accounted in the GW-Bethe-Salpeter (GW-BSE) calculation, one can see a red shift in the peak position from 5.2eV to 4.6eV [17].

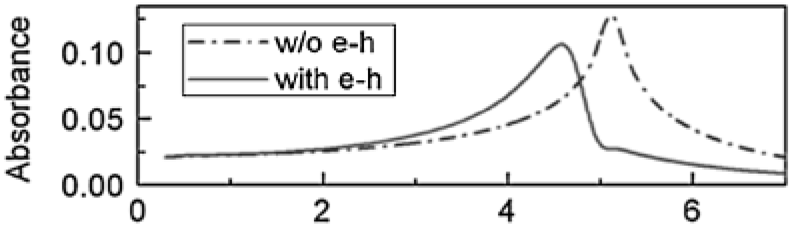

Figure 1.19 –Theoretical absorbance of graphene calculated with and without the calculation of e-h interaction. From [17].

Figure 1.19 shows that there is a uniform absorbance at approximately 0.5-1.5eV, which is supported by the experimental work mentioned above. Also, this theoretical results show that there is a significant influence of many body effects in graphene. Due to the vanishing density of states at the Dirac point, the screening of Coulomb interaction between the carriers are significantly reduced. Thus, the inclusion of e-e and e-h interaction in graphene is very important [17,21,20,22]. The curve (theoretical absorbance with e-e interaction but without e-h interaction)that peaks at 5.2eV assumes a symmetrical shape at the peak and this peak is due to band to band transition near the saddle point singularity, M point shown in Figure 1.15. At this singularity point, the joint density of states (JDOS) is proportional to $-\log|1-(\omega/\omega_0)|$, which is symmetrical near the singularity point [21-22]. Since optical conductivity is related to JDOS, the conductivity will also assume a symmetrical shape.

However, with the include of the e-h interaction in the GW-BSE calculation, the oscillator strength is re-distributed from higher energy to lower energy at around 4.6eV and the shape of the shifted peak assumes an asymmetry shape. This re-distribution has been observed experimentally in [21-22]. Not only do we see the red shift experimentally, we can also see the asymmetric red-shifted peak.

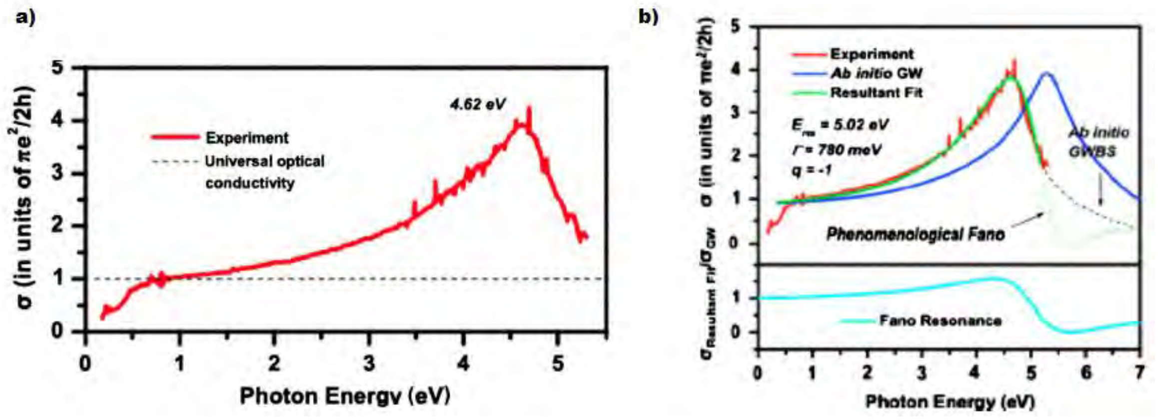

Figure 1.20 – a) Experimental optical conductivity of graphene on SiO2/Si b)Fano fitting of experimental conductivity. From [21].

The redistribution of oscillator strength (red-shift) can be explained by an exciton resonance at an energy below the saddle point singularity such that the discrete excitonic states couples strongly and reside within the existing continuum of states. U.Fano [23] mentioned that the interference of the discrete states with the continuum states will give rise to an asymmetric peak. Thus, a Fano fitting is normally carried out to the red shifted conductivity spectrum using the following equation:

$$\frac{\sigma(E)}{\sigma_{CONT}\ (E)} = \frac{(q+\varepsilon)^2}{1+\varepsilon^2} \qquad (1.66)$$

Where $\sigma_{CONT}\ (E)$ refers to the optical conductivity arising from the unperturbed band to band transition (only GW calculation that includes e-e interactions), $\varepsilon=(E-E_{res})/(\Gamma/2)$, where Γ is the width of the perturbed conductivity curve (with e-h interaction) and E_{res} is the resonance energy. Also, the parameter q^2 defines the ratio of the strength of the excitonic transition to the unperturbed band transitions while the sign of q will determine the asymmetry of the line shape [21,23]. The inset in Figure 1.20b shows the respective values used to Fano-fit the experimental conductivity curve. It is noteworthy to mention that the width parameter Γ used from reference [21] is 780meV, which corresponds to an excitonic lifetime of only ~ 0.5fs, from the Heisenberg‟s uncertainty principle. This suggested an extremely short lifetimes for the resonant excitons, which requires more study and research to understand the reason.

1.3 MOTIVATION OF THESIS

The above theory for the excitonic effects of free-standing graphene sets the motivation our thesis. In this thesis, we want to study graphene on SiO2/Si using spectroscopic ellipsometry, in order to see how the excitonic effects vary when compared with the conductivity spectrum to a free standing graphene shown in Figure 1.19. The results will be important for theoretical development and practical photonic devices usage, especially for graphene on SiO2/Si, a widely used substrate material.

CHAPTER 2 SPECTROSCOPIC ELLIPSOMETRY AND SIMULATION

Our experiment is carried out using Sentech SE850 rotating analyzer with compensator ellipsometer (PCSA$_R$). This chapter is catered to introduce our experimental technique, the experimental set-up, in particular the quantities that are measured, the mathematics behind ellipsometry as well as a justification on why ellipsometry is a suitable experimental technique for our experiment.

2.1 EXPERIMENTAL PROCEDURES

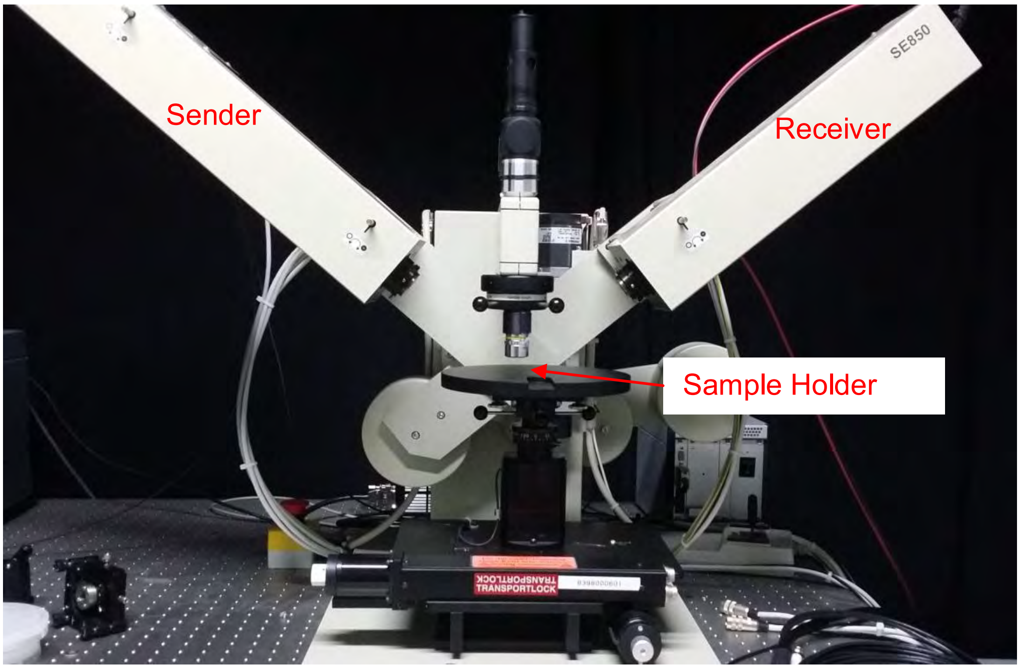

Figure 2.1 – Ellipsometer set-up.

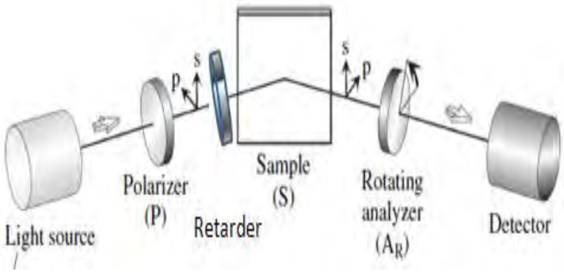

Figure 2.2 – Components of PCSA$_R$. From [3].

The Figure 2.1 above shows the equipment used. The sender sends the light to the sample placed on the sample holder, and the receiver will receive the light reflected off the sample. Our equipment consists of three light sources: Halogen Lamp that provides infrared from 0.5-1.5eV ,Xenon Lamp that provides visible light to UV from 1.5-4.8eV and Deuterium lamp that provides deep UV light from 4.8-6.5eV. From Figure 2.2, we see an illustration of the components of the ellipsometer used. It consist of a polarizer, rotated and fixed at 45^0 , and a retarder. After light reflected off the sample, it will go through the rotating analyzer, followed by the detector.

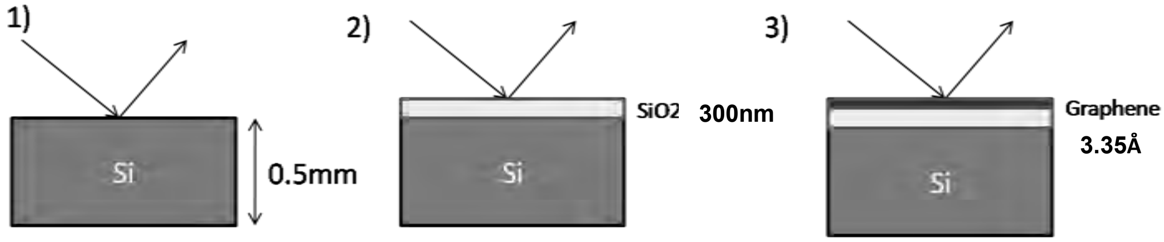

Figure 2.3 – Sequence at which experiment is conducted.

The experiment is done in a systematic manner: Si sample is first measured, followed by the SiO2/Si and lastly graphene on SiO2/Si. This is illustrated in Figure 2.3. Also, the three incidence angles of light were used, namely 50^0, 60^0 and 70^0 and this can be done by changing the angle of the „Sender". After which, the quantities Ψ and Δ will be measured. In the next section, we will be discussing the physical meaning of both Ψ and Δ. It should be mentioned that the samples Si and SiO2/Si were gotten from our manufacturer and SiO2/Si was grown through dry oxidation. As for the growth of graphene on SiO2/Si, it was conducted by Dr. Pranjal Gogoi in the clean room located at the Singapore Synchrotron Light Source (SSLS). Graphene grown on copper (Cu) foil was purchased from Graphene Square Inc, and from that, chemical etching was carried out to extract graphene.

2.2 QUANTITIES MEASURED – Δ,‎ Ψ

Upon light reflection off the sample, the P and S polarized light will differ significantly such that there will be changes to their amplitude ratio, Ψ and their phases, Δ. Ellipsometry measures these quantities.

In ellipsometry, it is defined that:

$$\rho = \tan\Psi \exp(i\Delta) = \frac{r_p}{r_s} = \frac{E_{rp}}{E_{ip}} \frac{E_{is}}{E_{rs}} \qquad (2.1)$$

where the last term is due to Equation (1.44) and Equation (1.45). E_{ip}, E_{rp}, E_{tp} represents the amplitude of E field of incident, reflected and transmitted P polarized light while the subscript s represents that of S- polarized light and r_p and r_s are the Fresnel"s equations, as defined in Section 1.18.

If E_{is}=E_{ip} (linearly polarized light), then from Equation (2.1),

$$\Delta = \delta_{r_p} - \delta_{r_s} \qquad (2.2)$$

and

$$\tan\Psi = \frac{|E_{rp}|}{|E_{rs}|} = \frac{|r_p|}{|r_s|} \qquad (2.3)$$

Thus, from Equation (2.3), one can see that the quantity Ψ measures the angle determined from the ratio of the amplitude of r_p and r_s. Also, it is evident from Equation (2.2) , Equation (1.46) and Equation (1.47) that the quantity Δ measured is the phase difference between the P- and S- polarized light after reflecting off the sample.

Spectroscopy ellipsometry can be both a direct or indirect measurement method to measure the optical functions of sample. It is a direct method when the optical model used is just a single layer (or a 01 system).Meanwhile, for a multilayered optical model, one has to go through curve-fitting of the measured Ψ and Δ to extract the optical functions of sample. This will be elaborated in later sections.

2.3 MATHEMATICS OF ELLIPSOMETRY

In Section 2.1, it has been mentioned that Ψ and Δ are measured from an ellipsometer. In this section, the mathematics will be reviewed, so that we can understand how the ellipsometer measures those quantities.

Polarization state of light as well as each of the optical devices shown in Figure 2.2 can be represented with mathematical matrices called the Jones matrices. The table below shows a summary of the Jones matrices that will be used in this section.

Polarization state of light	Jones Matrix	Optical Devices	Jones Matrix
General:	$\begin{bmatrix} \mathrm{E_{xo}} \exp(\mathrm{i}(\delta_x - \delta_y) \\ \mathrm{E_{yo}} \end{bmatrix}$	Polarizer/ Analyzer,	$\begin{bmatrix} 1 & 0 \\ 0 & 0 \end{bmatrix}$
Linearly polarized light (parallel to x, y axis):	$\begin{bmatrix} 1 \\ 0 \end{bmatrix}, \begin{bmatrix} 0 \\ 1 \end{bmatrix}$	Compensator	$\begin{bmatrix} 1 & 0 \\ 0 & \exp(-\mathrm{i}\delta) \end{bmatrix}$
Linearly polarized light (45^o):	$\frac{1}{\sqrt{2}}\begin{bmatrix} 1 \\ 1 \end{bmatrix}$	Sample	$\begin{bmatrix} \sin\Psi \exp \mathrm{i}\Delta & 0 \\ 0 & \cos\Psi \end{bmatrix}$
Right Circularly Polarized Light:	$\frac{1}{\sqrt{2}}\begin{bmatrix} 1 \\ i \end{bmatrix}$		
Left Circularly Polarized Light:	$\frac{1}{\sqrt{2}}\begin{bmatrix} 1 \\ -i \end{bmatrix}$		

Table 1: Summary of Jones matrix

In Table1, one can get the Jones matrix of a right circularly polarized light, simply by substituting $\delta_y = \pi/2$ and $\delta_x = 0$. This means that when the phase difference of light is known, one can represent it with the Jones matrix. Also, in Table1, the compensator is represented by

$\begin{bmatrix} 1 & 0 \\ 0 & \exp(-\mathrm{i}\delta) \end{bmatrix}$. The compensator is placed in front of the polarizer shown in Figure 2.2 such that it is used to convert the linearly polarized light into circularly polarized light or vice versa. In order to do that, the compensator is composed of a birefringent crystal, such that the refractive index, n is different in different axis of the crystal. In the fast or extraordinary axis, the refractive index is represented by n_e. Meanwhile, in the slow or ordinary axis, the refractive index is represented by n_o and $n_o > n_e$. From Equation (1.12), light waves that are parallel to the slow or ordinary axis will travel slower that light waves parallel to the fast or extraordinary axis. Since light travels with different speed inside the compensator, they will end up with a different phase. Hence, in Table 1, $\delta = \frac{2\pi}{\lambda} |n_e - n_o| d$, is the phase difference generated and d is the thickness of the compensator.

We now need to define the coordinate system of our system before describing the mathematics in proper. Before the reflection of light off a sample, δ_x will be $\delta_{E_{ip}}$ while δ_y will be $\delta_{E_{is}}$. After reflection, δ_x will be δ_{r_p} while δ_y will be δ_{r_s}. This is illustrated in the following figure.

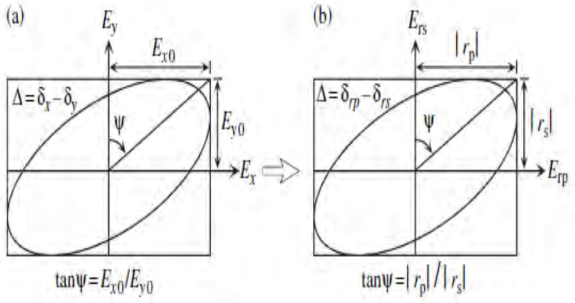

Figure 2.4 – Coordinate representation of a) the (E_x,E_y) axis and b) (E_{rp},E_{rs}) axis. From [3].

For convenience purposes, the matrices represented by different optical devices listed in Table1 will be labeled according to their first alphabet; matrices of polarizer/ analyzer are labeled as P and A respectively, compensator and sample matrices are labeled as C and S respectively.

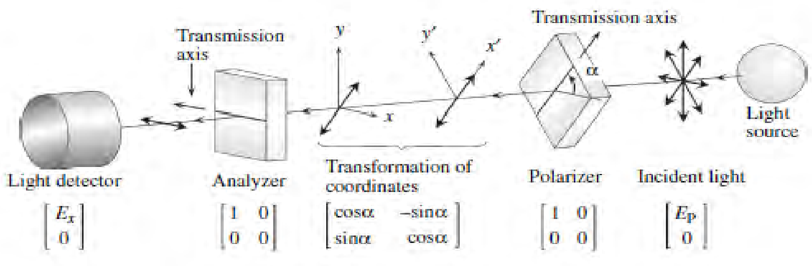

Figure 2.5 – An example of how the matrices work. From [3].

A simple example of how the matrices multiplication works is first shown, before evaluating for our experimental set-up. From Figure 2.5, light is first transmitted into the polarizer which has an angle α, defined positive if it is tilted counter-clockwise from the x (or the E_{ip} axis) when looked against the propagation direction of light. In this case, when light is transmitted out from the polarizer, it is in a x^l and y^l coordinate system such that x^l is the transmission axis of the polarizer, hence, there is a need to change the coordinate system of the light vector coming out of the polarizer, to match the coordinate system where x axis= E_{ip} and y axis = $E_{is.}$ To do this, we apply a rotation matrix, R(-α) to the multiplication, such that R(α)=$\begin{bmatrix} \cos\alpha & \sin\alpha \\ -\sin\alpha & \cos\alpha \end{bmatrix}$. R(α) represents a counter - clockwise rotation of the coordinate system (when looked against the propagation direction of light) and α is the positive angle of the polarizer. Then, light enters the analyzer. Supposed the analyzer is rotated at an angle a, then light vector has to be multiplied to the rotation matrix R(a), followed by the Jones matrix of analyzer, and finally, R(-a) in order to change the coordinate system of the light vector. To summarize, the matrix multiplication of the above system is represented as such:

$$L_{out} = R(-a)AR(a)\,R(-\alpha)PR(\alpha)L_{in} \tag{2.4}$$

where, S,P and A are the Jones matrix of the sample, polarizer and analyzer shown in Table 1 and L_{out} is the Jones vector of light detected. Equation (2.4) can be further simplified for our case; L_{in} cannot be represented with Jones vector, since it is an unpolarised light but we all know the fact that light is in the transmission axis (or the x^l axis)of the polarizer when it propagates out from the polarizer. $PR(\alpha)L_{in}$ from Equation (2.4) can now be simplified into the $\begin{bmatrix}1\\0\end{bmatrix}$. Also, since the light detector has no preference for the coordinate system that the light is in, R(-a) from Equation (2.4) can be dropped. Hence, Equation (2.4) can now be simplified as:

$$L_{out} = AR(a)R(-\alpha)\begin{bmatrix}1\\0\end{bmatrix} \tag{2.5}$$

Applying these knowledge to our experimental set-up in Figure 2.2, the Jones vector of the light detected can be represented as:

$$\begin{aligned} L_{out} &= \begin{bmatrix}E_A\\0\end{bmatrix} \\ &= \begin{bmatrix}1 & 0\\0 & 0\end{bmatrix}\begin{bmatrix}\cos\alpha & \sin\alpha\\-\sin\alpha & \cos\alpha\end{bmatrix}\begin{bmatrix}\sin\Psi\exp(i\Delta) & 0\\0 & \cos\Psi\end{bmatrix}\begin{bmatrix}e^{-i\delta} & 0\\0 & 1\end{bmatrix}\begin{bmatrix}\cos P & \sin P\\-\sin P & \cos P\end{bmatrix}\begin{bmatrix}1\\0\end{bmatrix}\end{aligned} \tag{2.6}$$

Note that the notation has been changed. α is the angle of analyzer while P is the angle of polarizer.

Since the angle of the polarizer, P is 45^0 , Equation (2.6) can be simplified into:

$$\begin{bmatrix}E_A\\0\end{bmatrix} = \begin{bmatrix}1 & 0\\0 & 0\end{bmatrix}\begin{bmatrix}\cos\alpha & \sin\alpha\\-\sin\alpha & \cos\alpha\end{bmatrix}\begin{bmatrix}\sin\Psi\exp[i(\Delta-\delta)]\\\cos\Psi\end{bmatrix} \tag{2.7}$$

and further simplified into:

$$E_A = \cos\alpha\sin\Psi\exp[i(\Delta-\delta)] + \sin\alpha\cos\Psi \tag{2.8}$$

The light intensity detected will be:

$$\begin{aligned} I = |E_A|^2 &= I_o(1-\cos2\Psi\cos2\alpha+\sin2\Psi\cos(\Delta-\delta)\sin2\alpha) \\ &= I_o(1-\cos2\Psi\cos2\omega t+(\sin2\Psi\cos\Delta\cos\delta+\sin2\Psi\sin\Delta\sin\delta)\sin2\omega t) \\ &= I_o(1+S_1\cos2\omega t+(S_2\cos\delta-S_3\sin\delta)\sin2\omega t)\end{aligned} \tag{2.9}$$

From Equation (2.9), we see that α=ωt, since the analyzer is rotating at a frequency of ω. S_1 and $(S_2\cos\delta-S_3\sin\delta)$ are known to be the Fourier coefficients of $\cos2\omega t$ and $\sin2\omega t$

respectively. These Fourier coefficients are computed by the equipment, using the principle of Hadamard transform, a Fourier analysis mentioned in [24]. Once S_1 is gotten, the quantity Ψ can be measured. Also, Δ can be found from $(S_2\cos\delta - S_3\sin\delta)$ calculated from the Hadamard transform, as different angles of incidence were carried out, as mentioned at the start of this section. Thus, we are able to read Ψ and Δ for our experimental data.

2.4 COMPARISON OF SPECTROSCOPY ELLIPSOMETRY WITH REFLECTANCE SPECTROSCOPY

In this section, my classmate Mr. Tay Shengyu and I worked very closely together to conduct a simulation to justify the use of spectroscopic ellipsometry. This simulation was aimed to compare the data analysis technique of reflectance spectroscopy as well as spectroscopy ellipsometry. Reflectance spectroscopy is a experimental set-up widely used, not just in the field of physics, but also in the field of medicine[25]. It measures the intensity of the reflected light off the sample (see Figure 2.6).

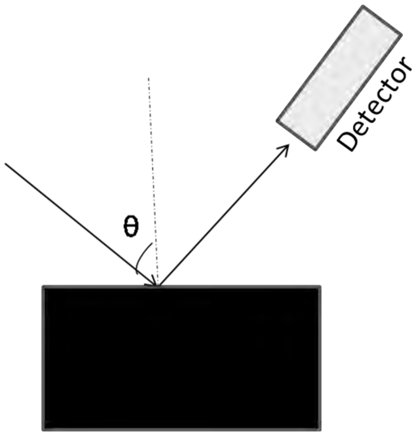

Figure 2.6 – Reflectance experiment for a single layer (optical model 01) system.

We simulated the reflectance curve of a sample (optical model 01 such that medium 0 is always the air, and medium 1 is the sample) measured by a reflectometer with energy limit till 7eV with normal incidence. Figure 2.7 shows our simulation of the reflectance curve.

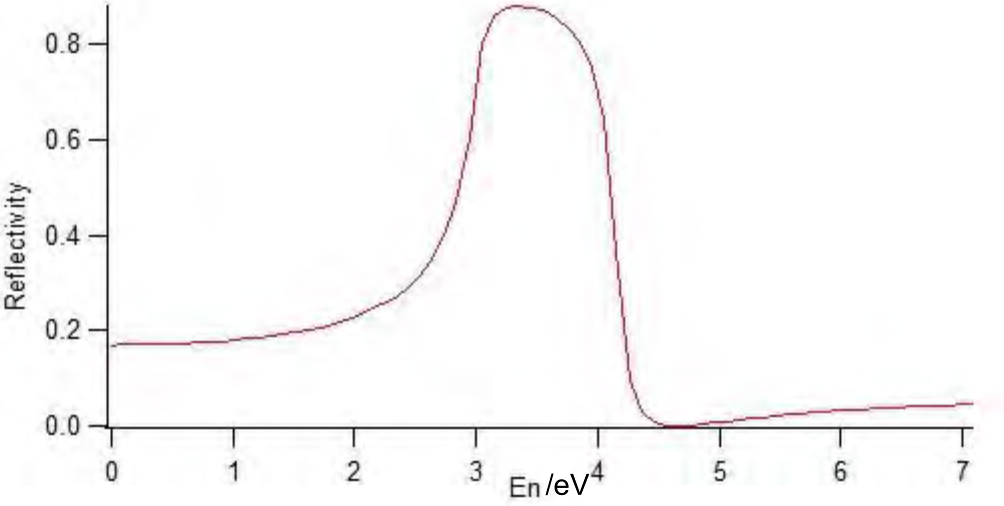

Figure 2.7 – Graph of simulated reflectance versus energy measured by reflectance spectroscopy, with energy limit at 7ev and normal light incidence.

In order to find the corresponding dielectric function ε(ω) of this reflectance curve, the following equations are used [7-8,26-27] . Since ε is related to R by the following relation at normal incidence:

$$r = \frac{1-\sqrt{\varepsilon}}{1+\sqrt{\varepsilon}} = \sqrt{R}\exp(i\Theta) \tag{2.10}$$

Where r is the reflection coefficient and Θ is the phase difference between the measured reflectance, R and reflection coefficient r. We can then write (2.10) in the following form :

$$\ln r(\omega) = \ln\sqrt{R(\omega)} + i\Theta(\omega) \tag{2.11}$$

Whereby Θ(ω) is the Hilbert Transform of ln $\sqrt{R(\omega)}$.

$$\Theta(\omega) = \frac{1}{\pi} P \int_{-\infty}^{\infty} \frac{\ln\sqrt{R(x)}}{x-\omega} dx \tag{2.12}$$

From Equation (2.12), it can be further evaluated into the following equations:

$$\Theta(\omega) = -\frac{2\omega}{\pi} P \int_{0}^{\infty} \frac{\ln\sqrt{R(x)}}{x^2-\omega^2} dx \tag{2.13}$$

and

$$\Theta(\omega) = -\frac{\omega}{\pi}\int_0^{\infty} \frac{\ln R(x) - \ln R(\omega)}{x^2 - \omega^2}\, dx \tag{2.14}$$

Doing an integration by parts on Equation (2.12) gives us:

$$\Theta(\omega) = -\frac{1}{2\pi}\int_0^{\infty} \frac{d}{dx}[\ln R(x)] \ln\left|\frac{x-\omega}{x+\omega}\right|\, dx \tag{2.15}$$

Both Equation (2.14) and (2.15) convenience our analysis of Θ, because of the absence of the principal value P. The strategy to extract the ε(ω) is as follows: we get Θ(ω) from the simulated R(ω) through the above equations, then go back to Equation (2.10) and do a inversion method to arrive to the dielectric function, ε of the sample simulated.

Note that the integration in Equation (2.14) are done from 0 to infinity, but in practice, we do not have high energy values to perform this. Following the work from reference [27], supposed our experiment is carried out with an energy limit from 0<E<b, then we will have to extrapolate for E>b. Equation (2.15) comes in useful as it shows that if d/dx(ln R(x)) =0, it does not contribute to the integral and this means that the R curve can be extrapolated as a constant, such that R=R(b).

The solving of Equation (2.14) is an arduous journey as almost a month was spent to figure out the computer codes to solve this integral. Finally, the integral was solved analytically using Mathematica. Having the values of Θ(ω), the dielectric functions were evaluated using Equation (2.10) and another program IGOR was used to generate the dielectric curves shown below.

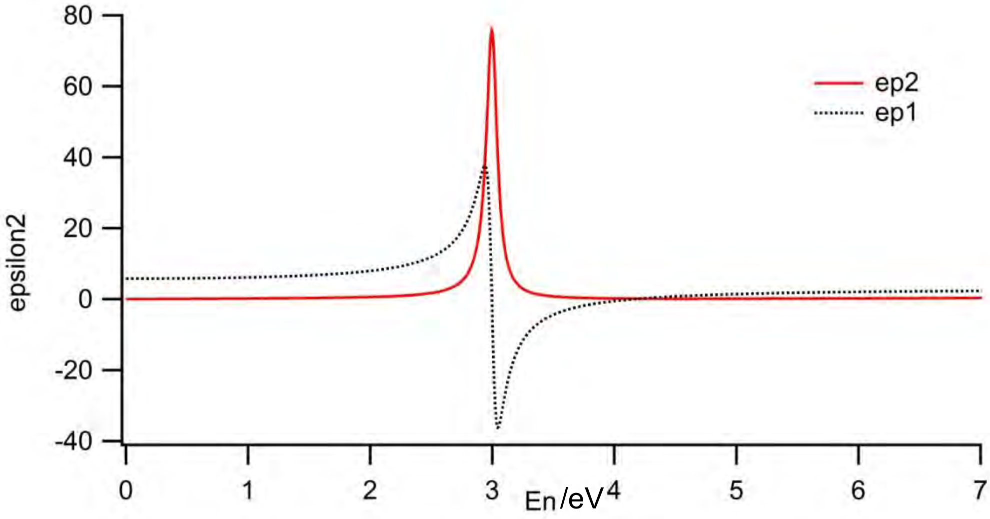

Figure 2.8 – Graph of ε_2 versus energy, extracted from simulated reflectance spectrum,

This particular data analysis method in reflectance spectroscopy is inaccurate as the simulated reflectance curve has to be extrapolated to a constant value (R @ 7eV)) outside the experimentally accessible energy range of 7eV. This gives rise to a large uncertainty (will be shown soon). By taking this extrapolation, we are making a big assumption that there is no more adsorption peak after 7eV, hence no more peak in epsilon 2 curve after 7eV.

Consider the scenario where the same sample is examined with a reflectometer of energy limit of 10eV, and it turns out that this sample also has an absorption peak at 8eV that is not detectable by the first simulation with energy limit of 7eV.

The reflectance curve is simulated to be:

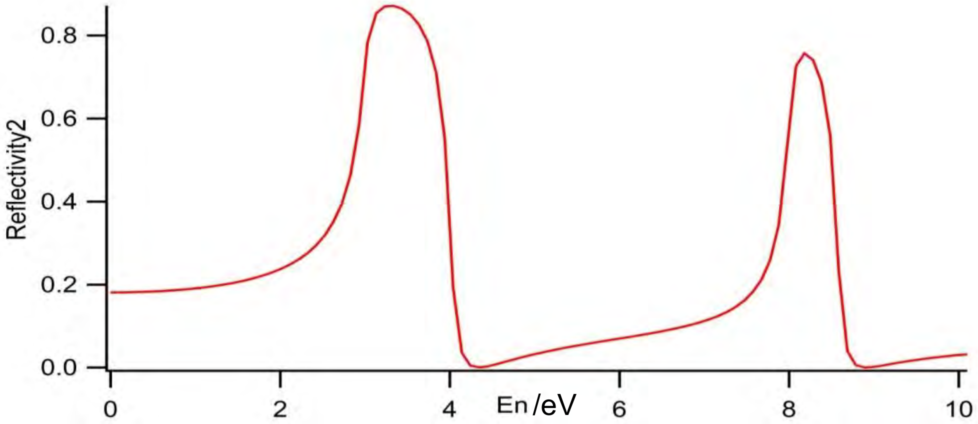

Figure 2.9 – Graph of simulated reflectance versus energy measured by reflectance spectroscopy, with energy limit at 10ev and normal light incidence.

Following the same procedure described earlier, we can generate the dielectric curves to be:

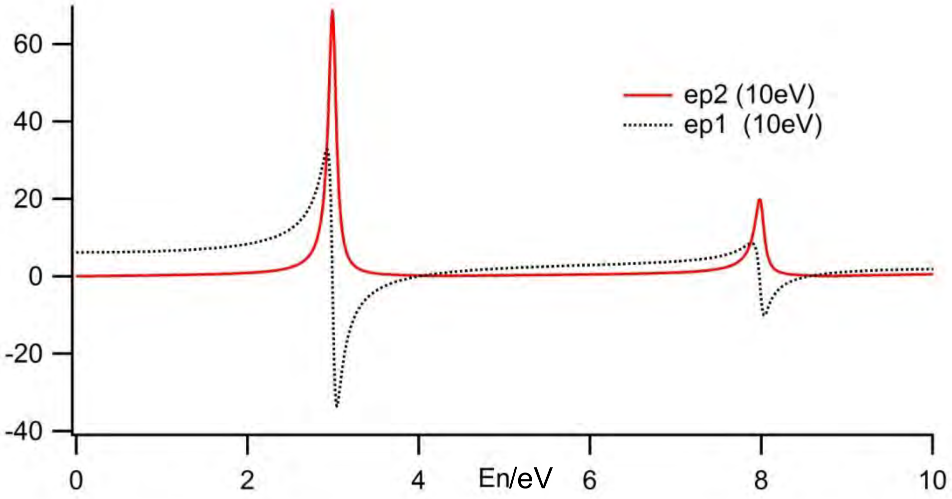

Figure 2.10 – Graph of ε_2 versus energy. 10ev reflectometer is used.

If we compare Figure 2.8 and Figure 2.10 in Figure 2.11 below, we conclude that Kramers-Kronig can be rather inaccurate. At energy less than 7eV, the ε_2 from both experiments does not match each other , except maybe far from the absorption region. At 3eV, simulation1 (7eV) ε_2 curve has an amplitude of 76.153 while simulation 2 ε_2 curve(till10eV) has an amplitude of 68.677, giving a percentage difference of 10.3%.

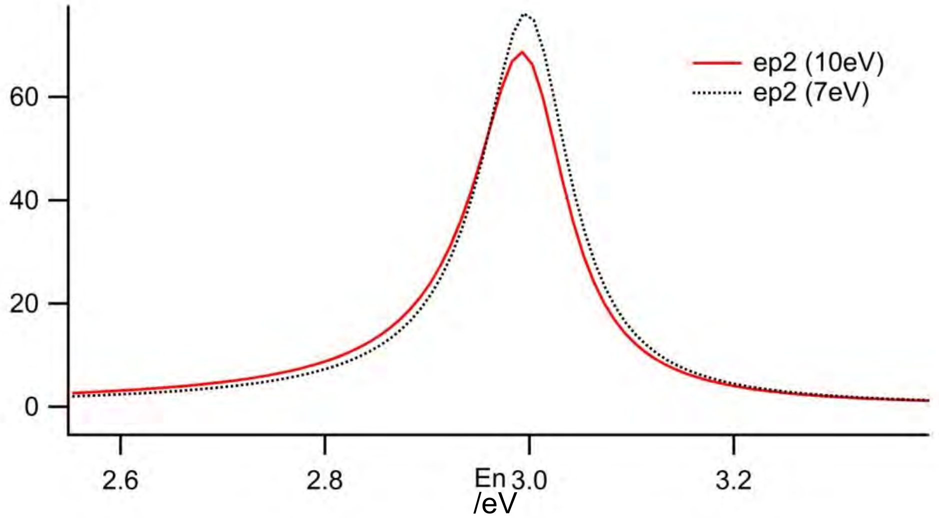

Figure 2.11 – Comparison of ε_2 curves generated by energy limit 7ev and 10ev reflectometer.

Although our reflectance spectroscopy simulation is done for normal incidence of light, the same idea still be forwarded for a varying incidence angles of light [28], such that the same Kramers Kronig analysis will still apply, thus giving the same kind of inaccuracy.

Meanwhile, in comparison, for a single layer of sample (01 optical model) shown in Figure 2.6, the spectroscopy ellipsometry will give more accurate results.

Equation (1.44) and Equation (1.45) shows that:

$$r_p = \frac{E_{rp}}{E_{ip}} = \frac{N_t \cos\theta_i - N_i \cos\theta_t}{N_t \cos\theta_i + N_i \cos\theta_t} \tag{2.16}$$

and

$$r_s = \frac{E_{rs}}{E_{is}} = \frac{N_i \cos\theta_i - N_t \cos\theta_t}{N_i \cos\theta_i + N_t \cos\theta_t} \tag{2.17}$$

such that Θ_i and Θ_t are the incident and transmitted angles respectively and N_i and N_t are the refractive index for the medium 0 and medium 1 optical systems respectively. These quantities are all connected by Snell"s Law, such that $N_i \sin\Theta_i = N_t \sin\Theta_t$ and N are related to the dielectric function by Equation (1.22). Using these information, Equation (2.1) can be written as:

$$\rho = \frac{r_p}{r_s} = \frac{\sin^2\theta_i - \cos\theta_i \left[\frac{\varepsilon^{(1)}}{\varepsilon^{(0)}} - \sin^2\theta_i\right]^{1/2}}{\sin^2\theta_i + \cos\theta_i \left[\frac{\varepsilon^{(1)}}{\varepsilon^{(0)}} - \sin^2\theta_i\right]^{1/2}} = \tan\Psi \exp(i\Delta) \tag{2.18}$$

such that $\varepsilon^{(1)}$ and $\varepsilon^{(0)}$ are the complex dielectric functions of optical systems 1 and 0 respectively.

Since medium 0 is always defined as air, $\varepsilon^{(0)}=1$ and Equation (2.18) can be written

$$\varepsilon^{(1)} = \sin^2\Theta_i [1 + \tan^2\Theta_i \left(\frac{1-\rho}{1+\rho}\right)^2] \tag{2.19}$$

In this case, we can directly calculate the dielectric function of the single layer, since Ψ and Δ are directly measured by ellipsometry. This requires no integration or extrapolation, unlike the Kramers-Kronig relation used in reflectance spectroscopy. Hence, spectroscopic ellipsometry is gives a better data analysis technique.

However, data analysis is easy only for single layer (01 optical model). For a multilayer system like our sample (0123 optical model such that medium 0 is air, medium 1 is graphene, medium 2 is SiO2 and medium 3 is Si), curve fitting is required. This is elaborated in Chapter 3.

Spectroscopy ellipsometry is also very sensitive to ultrathin films below 10nm. This is due to the fact that spectroscopy ellipsometry measures Ψ and Δ, which will show a significant change even an ultra thin film is added. This can be further illustrated from work done in reference [29].

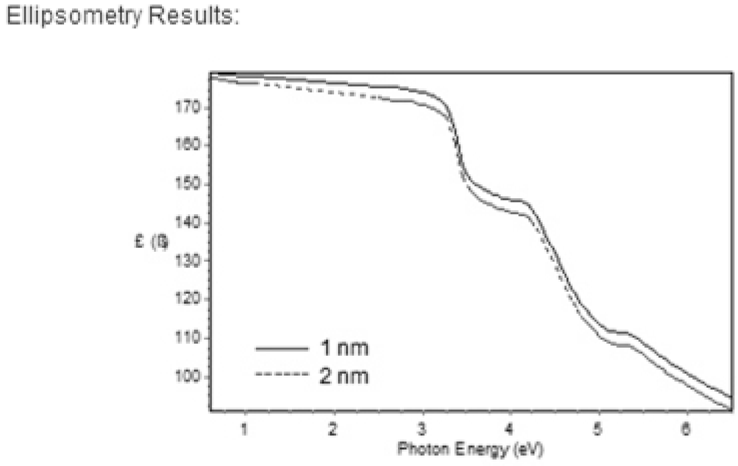

Figure 2.12 - Changes to Δ when thin film is added. From [29].

This feature of spectroscopy ellipsometry is very important for our experiment, as the graphene used has a thickness of atomic order (3.35Å). Overall, spectroscopy ellipsometry is a suitable experimental technique to be used.

2.4.1 DIFFICULTIES FACED IN THIS SIMULATION

As mentioned in the previous section, we took more than a month to finish the simulation. One of the strongest reasons for this delay is due to the wrong reflectance simulation. For more than half a month, me and my classmate Mr. Tay Shengyu used a lorentzian function to simulate the reflectance peak. When a lorentzian function is used, a unphysical ε_2 function will be gotten. From Equation (1.25) one should be aware that ε_2 must not be negative but the use of a lorentzian reflectance peak gives rise to negative ε_2. Failing to realize this mistake, my classmate and I thought that the problem lies with the Mathematica codes and we spent valuable time trying to rectify the Mathematica code that was already correct. However, it was after nearly one month and a half of communications over the Mathematica exchange forum and discussions with our supervisors that we found out that the use of lorentzian peak could be wrong. We then quickly rectified the reflectance equations to arrive at a physical ε_2 function.

2.5 SUMMARY

In this chapter, we have discussed the experimental procedures. We conducted the experiment in 50^0, 60^0 and 70^0 incidence angles and Si sample was first measured, followed by the SiO2/Si and lastly graphene on SiO2/Si, as illustrated in Figure 2.3. We then discussed the quantities measured in ellipsometry, such that the quantity Ψ measures the angle determined from the ratio of the amplitude of r_p and r_s, while the quantity Δ measured is the phase difference between the P- and S- polarized light after reflecting off the sample. These are described in Equation (2.2) and (2.3). We have went through the mathematics behind ellipsometry, and also created a simulation to argue that ellipsometry is suitable for our experiment because it requires no Kramer-Kronig relation and it is extremely sensitive to extremely thin sample. Lastly, it should be emphasized that spectroscopy ellipsometry can only work as a direct method when it involves a single layer (01 optical model) sample. Equation (2.19) shows that for a single layer sample, the dielectric function can be found directly from the measured Ψ and Δ. However, when it involves a multilayered system, curve fitting technique will be used to extract the dielectric functions. Curve fitting will be discussed in Chapter 3.

CHAPTER 3 : DATA ANALYSIS TECHNIQUE – CURVE FITTING

In the previous chapters, it has been mentioned that ellipsometry is an indirect method, such that curve fitting has to be done in order to get the desired dielectric functions ε_1 and ε_2 of our multilayered sample. However, this method does not need to be employed in the case of a single layer system (01 optical system), as discussed in Section 2.3. For a single layer, the dielectric function of medium 1 can be found directly from the following equation:

$$\varepsilon^{(1)} = \sin^2\Theta_i[1 + \tan^2\Theta_i\left(\frac{1-\rho}{1+\rho}\right)^2] \qquad (2.19)$$

such that $\varepsilon^{(1)}$ and $\varepsilon^{(0)}$ are the dielectric functions of optical system 1 and 0 respectively and Θ_i is the incident angle of light. Medium 0 is always air or vacuum.

It was also mentioned that the experiment is carried out in a systematic order. Firstly, medium 3, the Si is measured with the ellipsometer. Since it is a single layer, we can get the dielectric functions from Equation (2.19) . Then, SiO2 is grown on Si and measured with the ellipsometer. Of course, since this is a multilayered system, we have to employ the curve fitting technique to get the dielectric functions of SiO2 on a SiO2/Si system. Lastly, graphene is grown on the SiO2/Si substrates for measurements, so we do curve fitting again to extract the dielectric function of graphene on a SiO2/Si system.

3.1 CURVE FITTING

We shall now describe the curve fitting process, using the example of a SiO2/Si system. For a multilayered system with 012 optical system (air-SiO2-Si), the Fresnel"s equation is given in Section 1.1.8 to be:

$$r_{012,p} = \frac{r_{01,p} + r_{12,p}\exp(-i2\beta)}{1 + r_{01,p}r_{12,p}\exp(-i2\beta)}, \qquad (1.51)$$

$$r_{012,s} = \frac{\mathrm{r}_{01,s} + \mathrm{r}_{12,s}\exp(-\mathrm{i}2\beta)}{1 + \mathrm{r}_{01,s}\mathrm{r}_{12,s}\exp(-\mathrm{i}2\beta)}$$

such that $\beta = \frac{2\pi d_1 N_1}{\lambda}\cos\theta_1$ with Θ_1 as the transmission angles of light in medium 1. If Equation (1.51) is placed in the relation $\rho_{012} = \frac{r_{012p}}{r_{012s}}$, then one can see that $\rho=\rho(N_0,N_1,N_2,d_1,d_2, \Theta_0, \Theta_1, \Theta_2,\lambda)$. However, this can be shortened because of the Snell"s law, $N_0\sin\Theta_0= N_1\sin\Theta_1$. Also, according to Equation (1.22), $N^2=\varepsilon$. Hence,

$$\rho = \rho\left(\varepsilon^{(0)}, \varepsilon^{(1)}, \varepsilon^{(2)}, \mathrm{d}1, \mathrm{d}2, \Theta_0, \lambda\right) = \tan\Psi\exp(\mathrm{i}\Delta) \tag{3.1}$$

such that $\varepsilon^{(0)}, \varepsilon^{(1)}, \varepsilon^{(2)}$ are the dielectric functions in medium air, SiO2 and Si respectively.

We can already calculate $\varepsilon^{(2)}$ from Equation (2.19), thus essentially $\varepsilon^{(1)}$, the dielectric function of SiO2 is the only unknown in Equation (3.1). If we model the dielectric function of SiO2 with the Drude and Lorentz model described in Section 1.1.5, such that

$$\varepsilon = \varepsilon_\infty + \sum_i \frac{{\omega_{pi}}^2}{({\omega_{oi}}^2 - \omega^2) + i\gamma_i\omega} \tag{1.32}$$

then we can vary the parameters ω_p, ω_o and ϒ to fit our experimental Ψ and Δ.

Fortunately, these process can be done with this powerful program RefFit. The following figure shows a screen shot from this program.

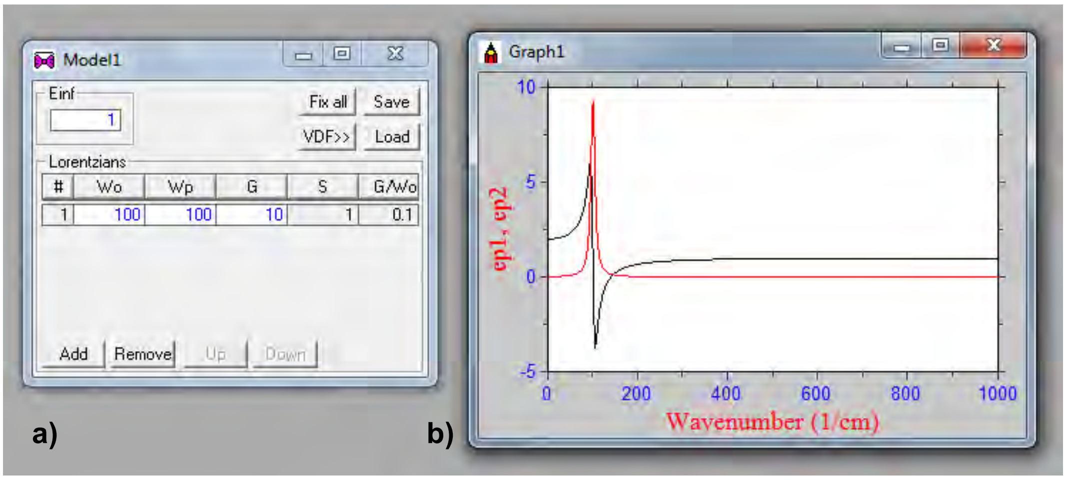

Einf

1

Lorentzians

#	Wo	Wp	G	S	G/Wo
1	100	100	10	1	0.1

Figure 3.1 – a) The model window in RefFit b) The graphs that is represented by Equation (1.32). From: A screenshot from RefFit.

On Figure 3.1a, it shows the parameters mentioned in Equation (1.32) while E_{inf} represents the ε_∞ and we can add oscillators by clicking on the “Add” button. Meanwhile, Figure 3.1b shows the corresponding ε_1 and ε_2 curves represented by Equation (1.32). RefFit offers some terrific built-in models for the users to fit data from ellipsometry, reflectance spectroscopy etc. We have used such a model (model -33) to do our curve fitting for Ψ and Δ and from there, we extracted the optical spectrum like dielectric functions.

Now it comes to the question of what gives a good fit. In practice, we visually inspect the fitting curves and the experimental curves, and make sure that they matches. However, this method can be dangerous as a „reasonably looking‟ match could be far from the numerically best curves. Thus we also employ a technique called “simultaneous fitting”. This means that we fitted 50^0, 60^0 and 70^0 data simultaneously, such that it really pin down to the unique dielectric functions. Also, we can calculate the “Mean Square Error” (MSE), and make sure they are minimized.

3.2 MEAN SQUARE ERROR

To calculate the fitting errors, we employ the use of unbiased estimator (or MSE) as shown below:

$$\sigma = \frac{1}{\sqrt{\mathrm{M}-\mathrm{P}-1}}\left\{\sum_{\mathrm{j}=1}^{\mathrm{M}}[\rho_{\mathrm{ex}}(\mathrm{E_j}) - \rho_{\mathrm{fit}}(\mathrm{E_j})]^2\right\}^{1/2} \tag{3.2}$$

where ρ is defined in Equation (2.1) and the subscripts ex and fit represents the experimental values as well as the fitting values. M refers to the number of experimental points while P refers to the number of fitting parameters [3].

Using Equation (2.1), we can further simplify the Equation (3.2) to become:

$$\sigma = \frac{1}{\sqrt{\mathrm{M}-\mathrm{P}-1}}\left\{\sum_{\mathrm{j}=1}^{\mathrm{M}}(\,[\tan\Psi_{\mathrm{ex}} - \tan\,\Psi_{\mathrm{fit}}]^2 + \;[\cos\Delta_{\mathrm{ex}} - \cos\,\Delta_{\mathrm{fit}}]^2\right\}^{1/2} \tag{3.3}$$

However, this technique of finding the fitting error is not perfect [30]. There are some flaws that are noteworthy to be mentioned. Firstly, the unbiased estimator does not give a clear indication or guideline to whether further fitting can result in a statistically minimum value. The best method is curve fit several times, and try to reach the lowest value of the unbiased estimator as possible. Secondly, the accurate parts and the inaccurate parts of the experimental spectrum are given the same weight, thus the final unbiased estimator calculated is high, even when it is visually a good fit. The experimental spectrum (See Chapter 4) fluctuates very badly in the infrared spectrum and the discrepancy for the Ψ and Δ measured at deep UV range also increases. This implies that the discrepancy between the fitted curve and the experimental curve are high in these energy range, thus contributing to a higher value of the unbiased estimator.

Meanwhile, there is another fitting error function proposed, called the biased estimator [3,30]. The function is given by:

$$\chi = \frac{1}{\sqrt{\mathrm{M}-\mathrm{P}-1}}\left\{\sum_{\mathrm{j}=1}^{\mathrm{M}}\left[\frac{\rho_{\mathrm{ex}}(\mathrm{E_j}) - \rho_{\mathrm{fit}}(\mathrm{E_j})}{\delta\rho(\mathrm{E_j})}\right]^2\right\}^{1/2} \tag{3.4}$$

such that $\delta\rho(E_j)$ represents the measurement errors from the ellipsometry devices. The above equation can be further simplified to:

$$\chi = \frac{1}{\sqrt{M-P-1}} \left\{ \sum_{j=1}^{M} ([\frac{\Psi_{ex}(E_j) - \Psi_{cal}(E_j)}{\delta\Psi(E_j)}]^2 + [\frac{\Delta_{ex}(E_j) - \Delta_{cal}(E_j)}{\delta\Delta(E_j)}]^2 \right\}^{1/2} \qquad (3.5)$$

where $\delta\Psi(E_j)$ and $\delta\Delta(E_j)$ represents the measurement errors at each Ψ and Δ. The use of above function can reconcile the flaws that are caused by the unbiased estimator. Firstly, $\chi \sim 1$ when the fitting is sufficiently good, while $\chi >> 1$ if the fitting is not good. When the measurement errors are overestimated, we get $\chi < 1$. Secondly, it is possible to increase $\delta\Psi(E_j)$ and $\delta\Delta(E_j)$ intentionally at the low and high energies, so a better representation of the errors in the inaccurate parts of the experimental spectrum can be given.

However, despite the flaws that we have mentioned, we continued to use the unbiased estimator. This is because our equipment fails to give us the measurement errors at each energy values. Instead, we only know that $\delta\Psi$ and $\delta\Delta$ are 0.10^0 and 0.20^0 respectively, independent of energy. Thus, it is unsuitable for the biased estimator to be used for our case. In order to reconcile the second flaw mentioned, we excluded the regions with high experimental discrepancies (high and low energy) in the calculation, which is also a common practice to do so [3].

Meanwhile there are some reasons discussed in literatures [3,30] to why a sufficiently low MSE cannot be reached.

1) The measured Ψ and Δ are measured inaccurately.
2) The optical model used in data analysis is inappropriate.

In Chapter 4, we will set a range of acceptable MSE values to define acceptable fitting. More will be discussed in Chapter 4 as we discuss our data.

3.2.1 EVALUATION ON THE CURVE FITTING METHOD

From Equation (3.1), the only unknown is the dielectric function of SiO2. One might question on why the curve fitting technique is chosen, instead of using numerical inversion method.(By numerical inversion, it means plugging all the known values into Equation (3.1) to find the only unknown).

The curve fitting method has several advantages.

1) Firstly, in a 012 or 0123 optical system, the thickness of the film is also a changing parameter to be played with in RefFit. Although we have known the thickness of the Si, SiO2 thin film to be 0.5mm and 300nm respectively (given to us by the manufacturers), there are bound to have experimental discrepancies in these values. As we vary these values in the curve fitting process, we are able to find the “actual” thickness. However, if the mathematical inversion method is used, a fixed value of thickness will have to be used.
2) Each of the oscillators added in Figure 3.1a has their physical meaning; they represent the dielectric polarizations in the sample and from the program RefFit, one can see how much contribution each oscillators has contributed to the dielectric function. However, the numerical inversion method does not allow this.

However, this technique is not perfect. There are some disadvantages to this.

1) Firstly, it is very time consuming. One has to devote time and effort to fit the experimental curve and try to find the lowest unbiased estimator. Sometimes, it is a game of trial and error, and there is no recipe to fitting perfectly and quickly. The fitting of the results of Si substrate and SiO2/Si had taken more than a month, and fitting graphene on SiO2/Si took even longer.
2) Secondly, there is no clear and obvious criteria on how many oscillators are really necessary. The parameters of oscillator 1 can still be adjusted even when oscillator 2 has been added, thus adding to the difficulty of curve fitting.

3) The construction of optical model is very important. Optical models constructed can directly affect the results. Sometimes a good fit cannot be achieved because of the wrong optical model used. In Chapter 4, we shall discuss more about optical models when the results of graphene of SiO2/Si is being discussed.

Meanwhile, the curve fitting method is still widely used for spectroscopy ellipsometry as the advantages of curve fitting outweigh the disadvantages.

3.3 SUMMARY

In this chapter, we have discussed about the technique of curve fitting and the error analysis. We used the unbiased estimator instead of the biased estimator, mainly because our equipment does not offer us a energy dependent measurement errors, $\delta\Psi(\mathrm{E_j})$ and $\delta\Delta(\mathrm{E_j})$. We have also evaluated on the technique of curve fitting, by comparing it with the numerical inversion technique. The curve fitting offers us insights on the strengths of the oscillators and allow us to find out the “actual” thickness of the samples. Lastly, the flow chart below will briefly summarize the discussions for the data analysis of spectroscopy ellipsometry

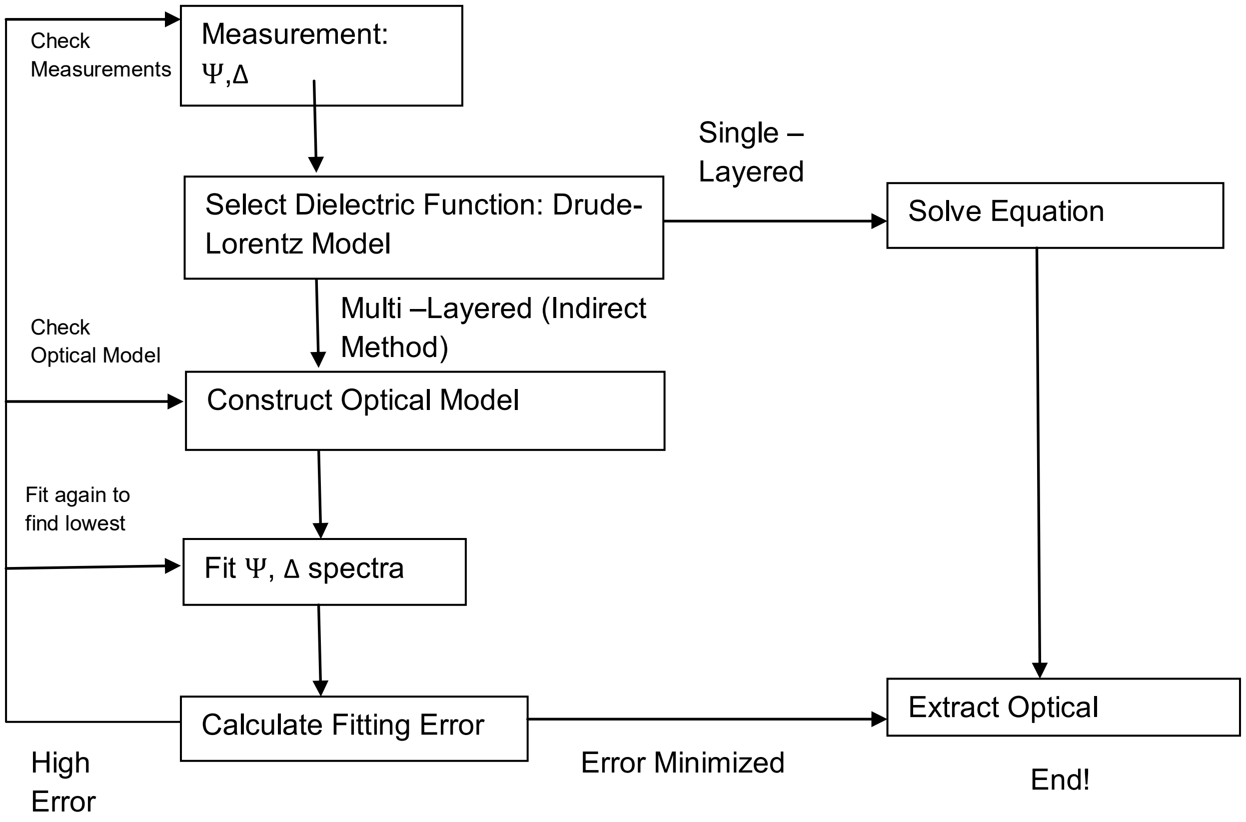

Figure 3.2 – Flowchart To Data Analysis Procedure In Spectroscopic Ellipsometry.

CHAPTER 4 EXPERIMENTAL RESULTS AND DISCUSSIONS

In this chapter, we will present the experimental results, the fitting as well as the optical functions extracted from the fitting and discuss their optical properties. We will also be looking at the unbiased estimator, and giving some suggestions to lower the value of the unbiased estimator. The results will be given in a systematic manner: Si first, followed by SiO2/Si and last but not least graphene on SiO2/Si.

4.1 RESULTS AND DISCUSSION FOR C-SILICON

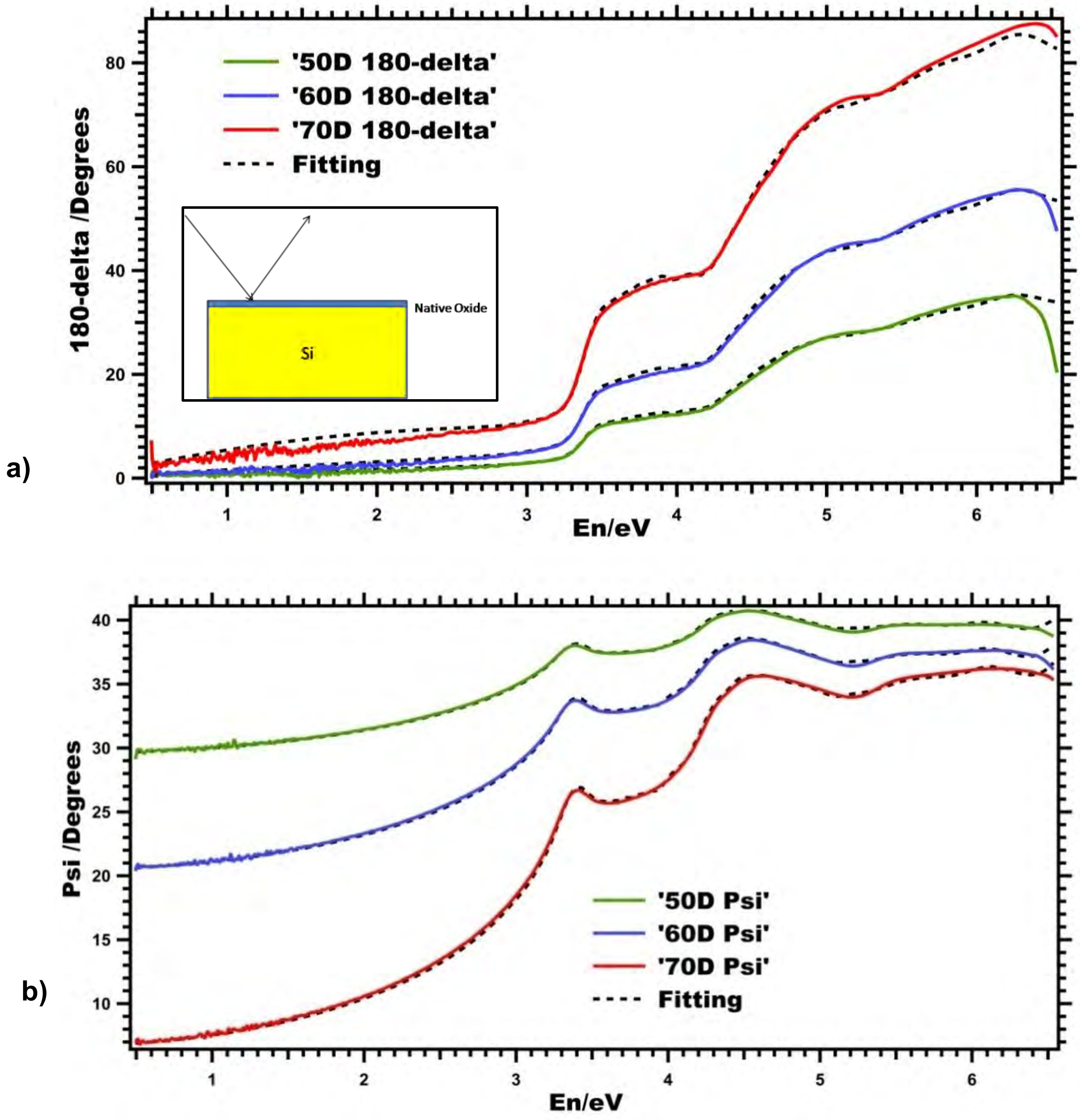

Figure 4.1 – a)) Experimental 180- Δ spectra for multiple incidence angles with fitting. b) Experimental Ψ spectra for multiple incidence angles with fitting. Inset: Optical model with native oxide.

We initially used a 01 optical model for this sample, where medium 0 is the air and medium 1 is the Si substrate. By using a 01 model, we are assuming that the system does not have any contamination. As mentioned in previous sections, being a single layered system, we can use Equation (2.19) directly to extract the dielectric functions. Using the experimental data for 70^0 Ψ and Δ as well as Equation (2.19), we calculated the dielectric functions and they are represented as the dotted lines in Figure 4.2.

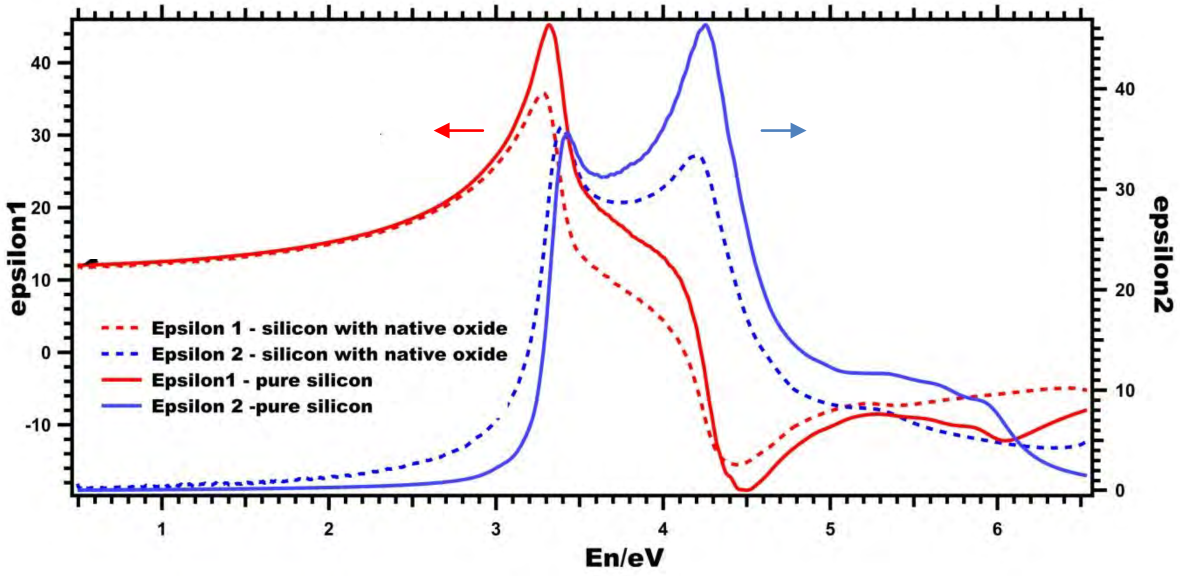

Figure 4.2 – Experimental Results. The red and blue dotted lines are calculated from Equation (2.19) with 70^0 data, while the filled lines are the dielectric functions extracted from curve fitting.

However, compared to the literatures [3,12-13], we see that the dotted lines in Figure 4.2 resembles a contaminated c-silicon instead of a pure c-silicon. One can see that the amplitude of ε_2 is lower than that of ε_1 with the high chance of a presence of native oxide. This suggests that we could have constructed the wrong optical model for the system. There is a very possibility that our c-silicon sample has been contaminated with a ultra thin layer of native oxide residing on top of it.

To rectify this, we constructed an optical model shown in the inset of Figure 4.1.

This is a 012 optical model, with air as medium 0, native oxide (SiO_2) as medium 1 and bulk Si as medium 2. By doing a simultaneous fit on the 50^0, 60^0 and 70^0 Ψ and Δ spectra in

Figure 4.1, we managed to extract the dielectric functions of a pure sample of c-silicon, which is shown as the filled lines in Figure 4.2.. From the fitting, we found the native oxide layer to be 2.24nm and the Si substrate to be 0.5mm. Table 2 below gives the unbiased estimator for each of the fittings. It must be mentioned that we do not include the fluctuations in the infrared regions (1.3eV and below) as well as high energy regions, from 6.1eV and above. As mentioned in Chapter 3, these regions are prone to have higher discrepancies. This is because these energies approach the energy limits of our equipment and there is lower amount of light intensity present in those regions.

Incidence Angles	Unbiased Estimator
70^0	0.00986^0
60^0	0.00568^0
50^0	0.00361^0

Table 2: MSE Values for curve fitting of Si.

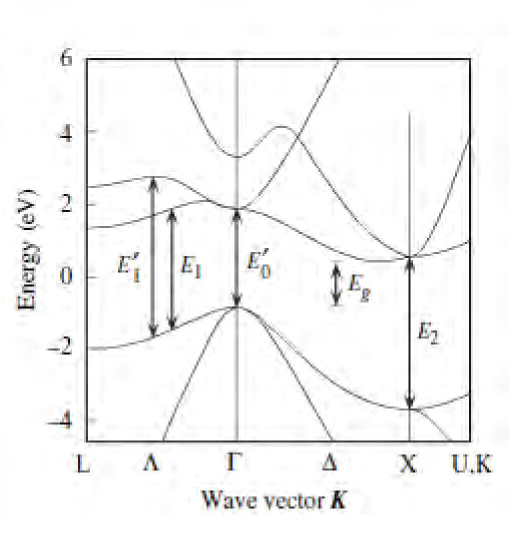

Figure 1.11 – Electronic Band Structure of Si. From [10].

In the ε_2 experimental spectrum shown in Figure 4.2, the optical transition of $E_o^{\backslash}$ and E_1 shown in Figure 1.11 is seen at the peak of 3.42eV, while the optical transition of E_2 is shown in the peak at 4.25eV. These agrees with the literatures presented in the Introduction section.

4.2 RESULTS AND DISCUSSION FOR SIO_2/SI

With the information of the dielectric function of c-Si, we are able to perform a curve fitting on the experimental results of the SiO_2/Si sample. Below shows the experimental results and their fitting. Inserted as an inset in the Figure is a picture of the optical model used and tabulated in Table 3 are the MSE values.

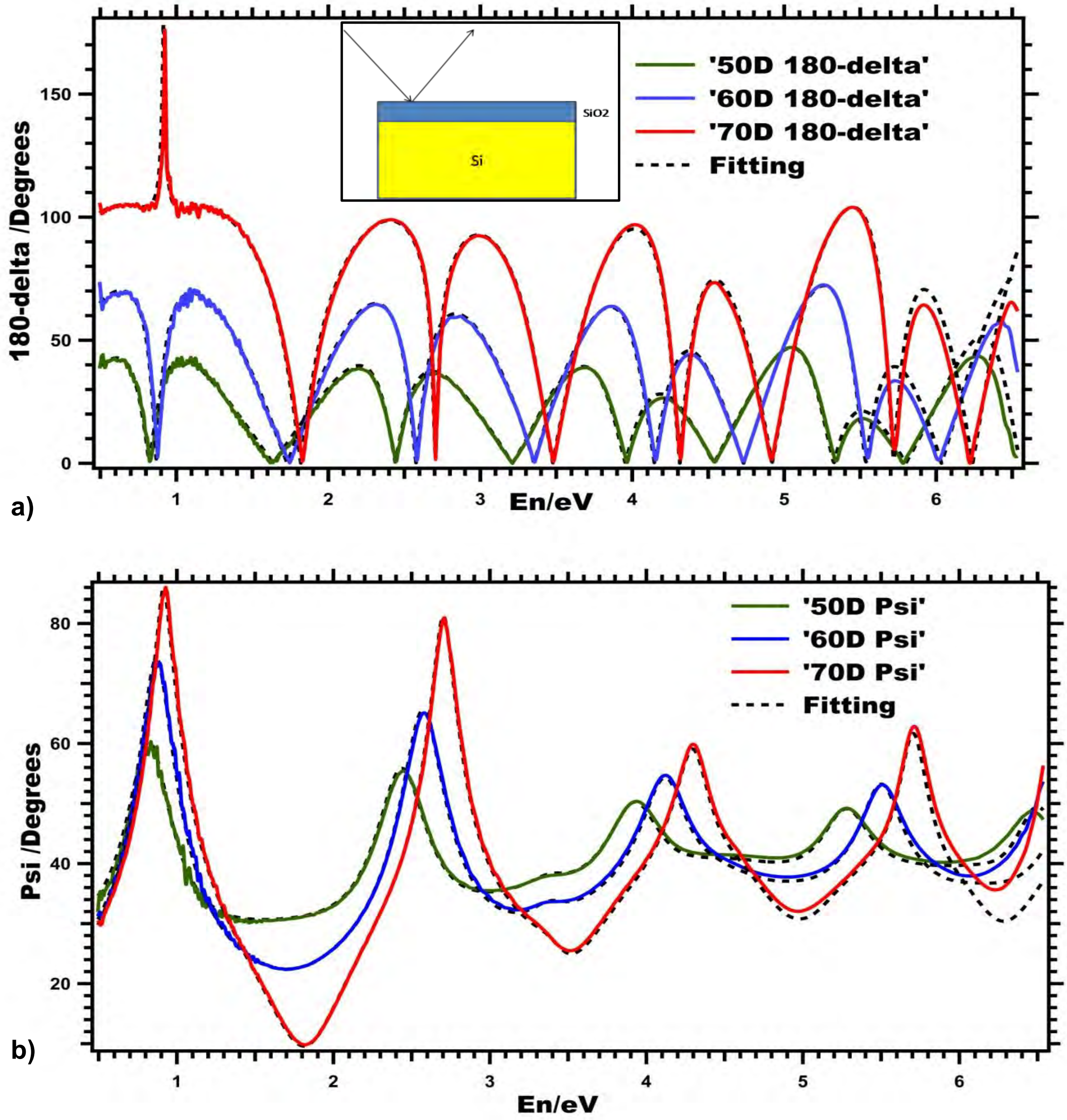

Figure 4.3 – a) The experimental (180- Δ) for multiple angles and fitting b) The experimental Ψ for multiple angles and fitting for SiO2/Si. Inset: Optical model used for fitting.

Incidence Angles	Unbiased Estimator
70^0	0.0407^0
60^0	0.0201^0
50^0	0.0132^0

Table 3: MSE Values for curve fitting of SiO2/ Si.

The following diagram is the extracted dielectric function of SiO_2 on Si.

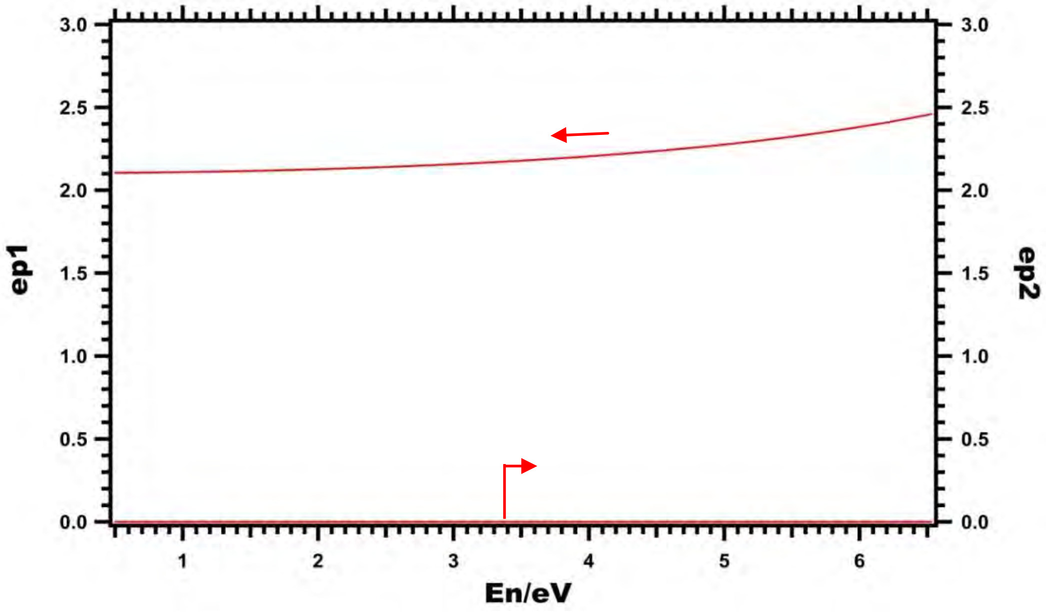

Figure 4.4 – Experimental Dielectric Function of SiO_2/Si.

The fitting was done with 307.48nm as opposed to the manufactured readings of 300nm. This clearly shows the advantage of curve fitting, being able to know the true thickness. From our results, we see that SiO2 is transparent in our experimental energy range since $\varepsilon_2 = 0$.

4.3 DETERMINATION OF AN ACCEPTABLE RANGE OF MSE

Before we show the results of the graphene on SiO2/Si, we need to first give a rough estimate of an acceptable MSE. We see from Table 2 and Table 3 the MSE calculated for each angles, and the corresponding dielectric functions agree well with other literatures. We now need to set a rough estimate for upper limit of MSE, such that beyond this value, we deem the fitting as a bad fitting.

To do that, we deliberately upset the fitting of Si curves and calculate the MSE values. This is shown in below figure.

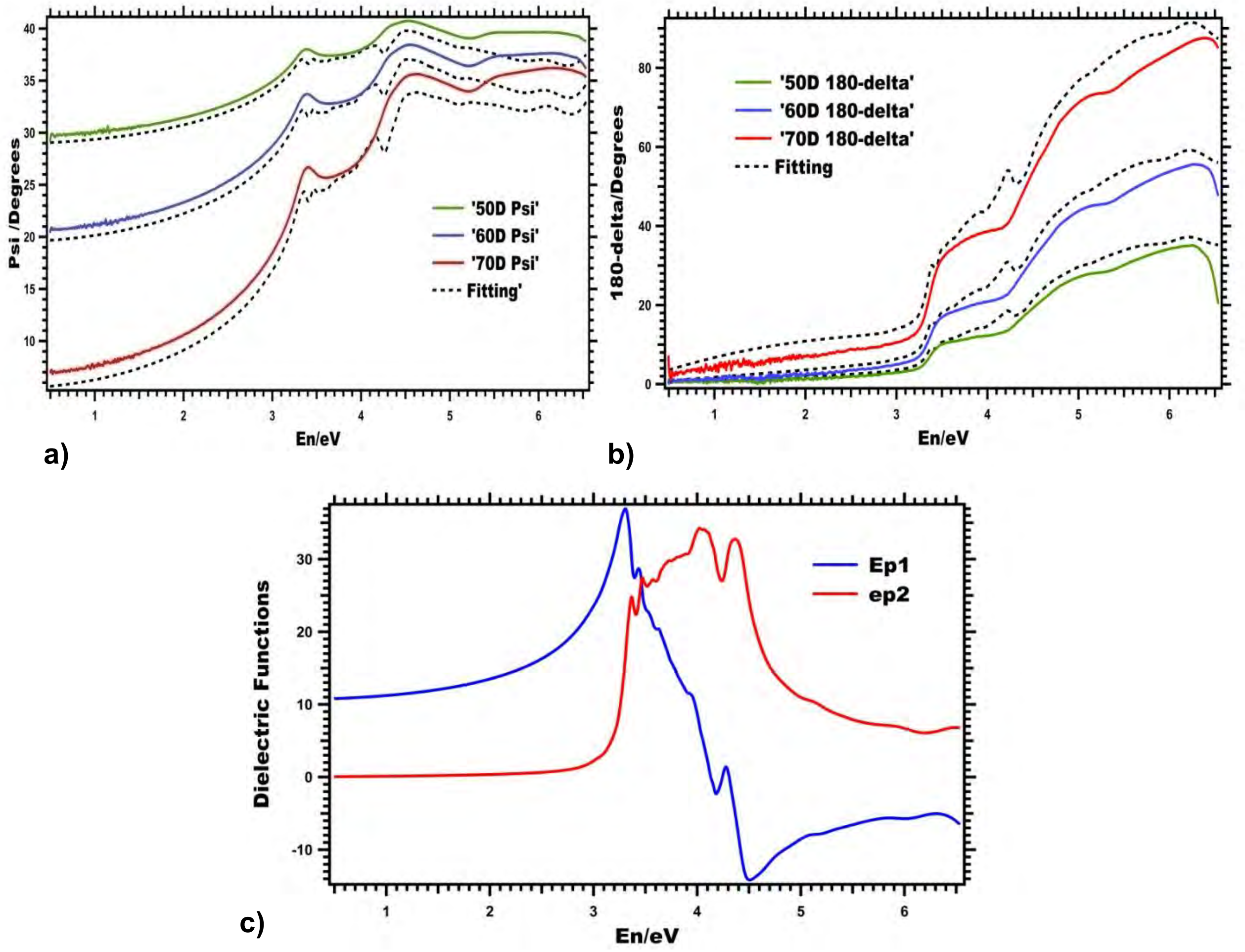

Figure 4.5 –An illustration of bad fitting. a) Ψ fitting for multiple angles. b) 180-Δ fitting for multiple angles. c) Corresponding dielectric functions.

Incidence Angles	Unbiased Estimator
70^0	0.0841^0
60^0	0.0638^0
50^0	0.0591^0

Table 4 – MSE tabulation

Clearly, the above fitting is not acceptable. Visually, we see that the curve fitting is not accurate. Looking at the corresponding Si dielectric functions, we see that it shows large deviations from other literatures. Hence, we give a rough estimate of the accepted range of the MSE – 0-0.0591^0. Beyond 0.0591^0, we shall deem the fitting to be unreasonable.

Once again, it must be emphasized that this only gives a rough estimation. We have to do this because the calculation of unbiased estimator does not give us the definition of what is a good fitting as mentioned in Chapter 3, and we needed a limit to check when a fitting is unreasonable.

4.4 RESULTS AND DISCUSSION FOR GRAPHENE ON SIO$_2$/SI

Now that the dielectric functions of SiO2 and Si are extracted, we are able to do the curve fitting on the Ψ and Δ measured. Once again, they are shown in figure below with the MSE values tabulated.

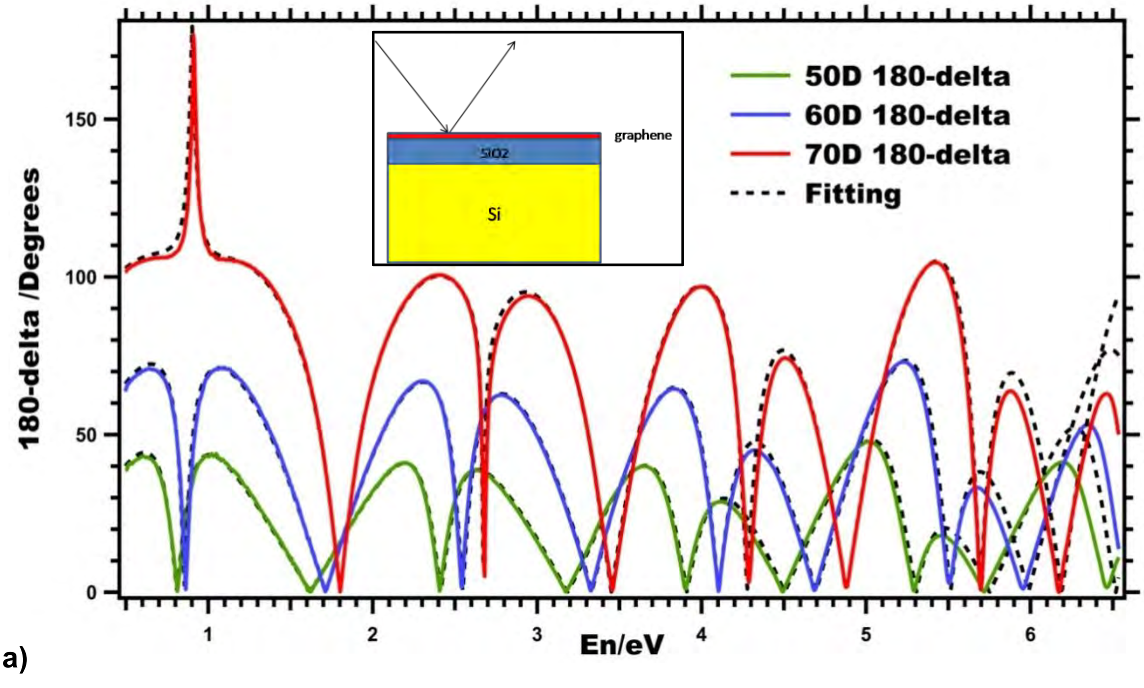

a)

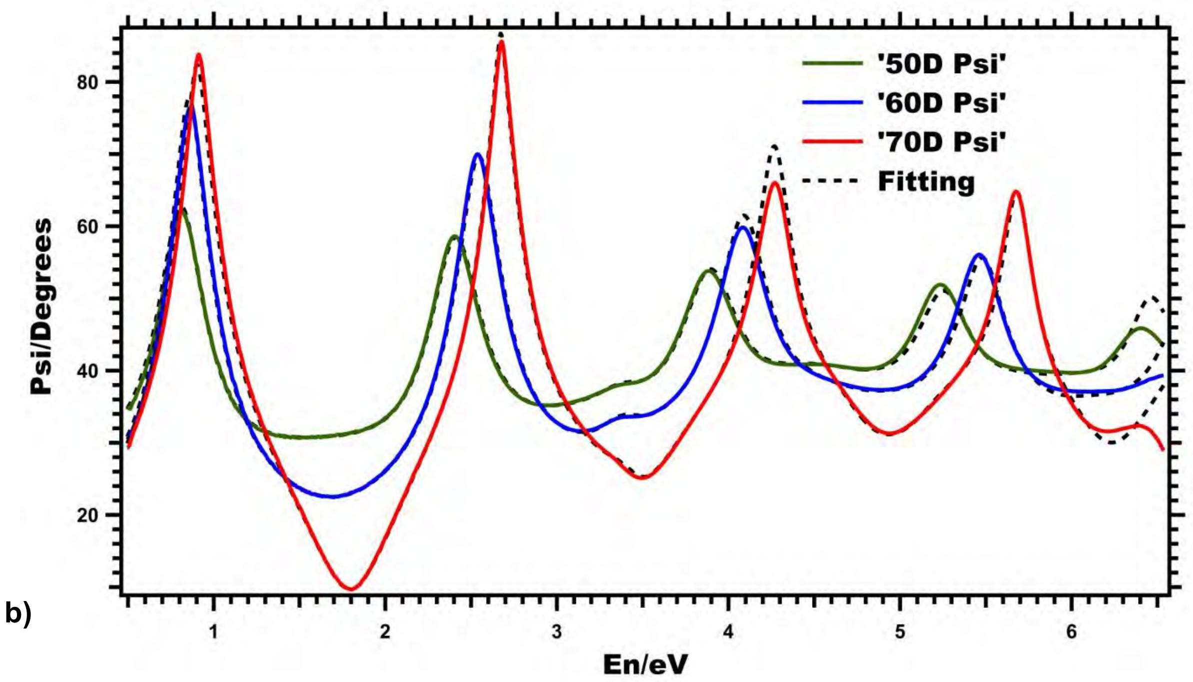

Figure 4.6 - a) The experimental (180- Δ) for multiple angles and fitting b) The experimental Ψ for multiple angles and fitting for Graphene on SiO2/Si. Inset: Optical model used.

Incidence Angles	Unbiased Estimator
70^0	0.289^0
60^0	0.0277^0
50^0	0.0165^0

Table 4: MSE Values for curve fitting of Graphene on SiO2/ Si.

Below shows the dielectric functions and conductivity of graphene on SiO2/Si extracted from the fitting.

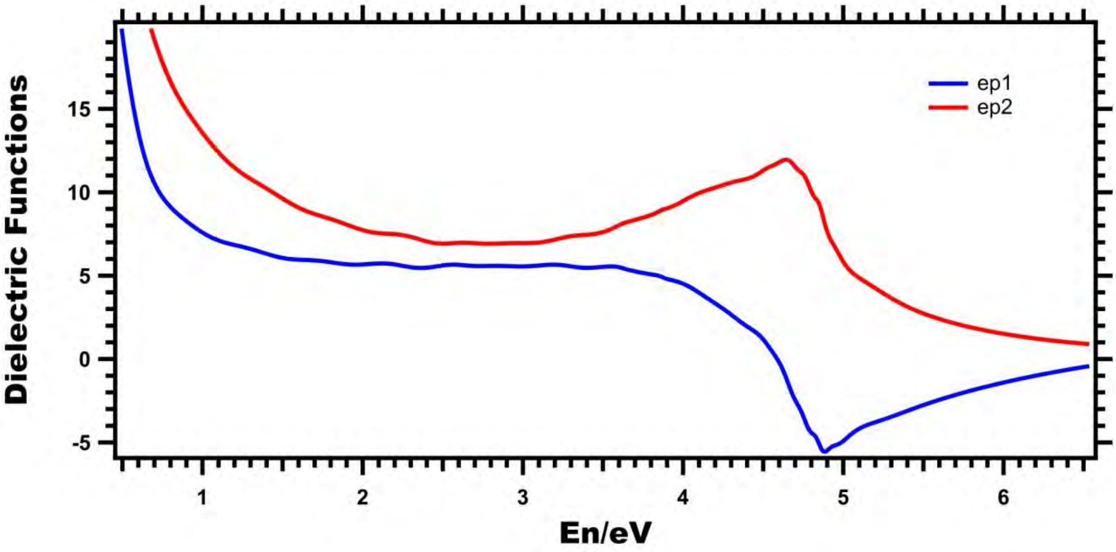

Figure 4.7- Experimental dielectric functions of graphene on SiO2/Si.

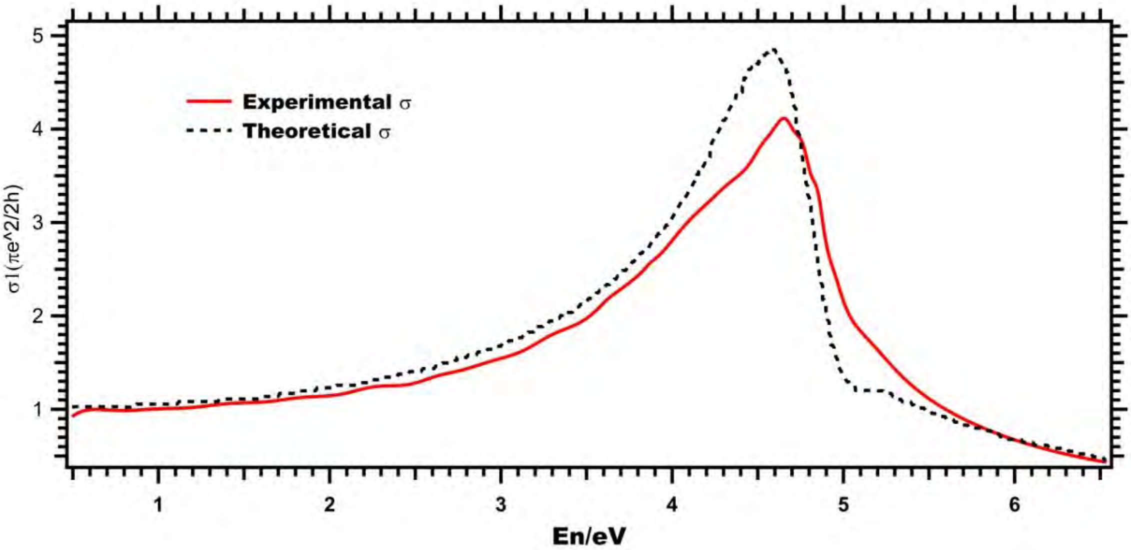

Figure 4.8 – Experimental optical conductivity of graphene on SiO2/Si with theoretical free-standing graphene extracted from [23] .

The fitting was done with 3.35Å of graphene layer. There are some traits to our experimental optical conductivity curve. Firstly, for low energy from 0.5-1.3eV, the conductivity is frequency independent and it is equal to the universal conductivity of $\frac{\pi e^2}{2h}$ which is in agreement with other literatures [17,19-22]. Secondly, the conductivity assume a asymmetrical peak, at 4.65eV, which is clearly due to the e-h interaction that is calculated in the GW-BSE calculations. The asymmetrical peak predicted and highlighted the importance of the resonant excitonic effects in the graphene. This asymmetry could also be explained by the Fano model, which suggested a discrete excitonic state residing within a continuum state.

In Figure 4.8, we have also compared the theoretical optical conductivity of free standing graphene with our experimental optical conductivity of graphene on SiO_2/Si. Upon comparison, there are two distinct features that should be noted.

1) There is a blue shift of the photon energy. The theoretical curve peaks at 4.60eV, while the experimental curve peaks at 4.65eV.
2) The experimental curve is less asymmetrical than that of the theoretical curve.

The above two observations could be due to two reasons.

Firstly, the optical model constructed might not be accurate and hence our corresponding experimental optical conductivity spectrum is inaccurate. Table 4 shows the MSE values determined from the fitting, and 70^0 fitting is unreasonable according to our guidelines. This high MSE value could be due to the incorrect optical model that was constructed. Below shows a series of optical modelling that could be constructed.

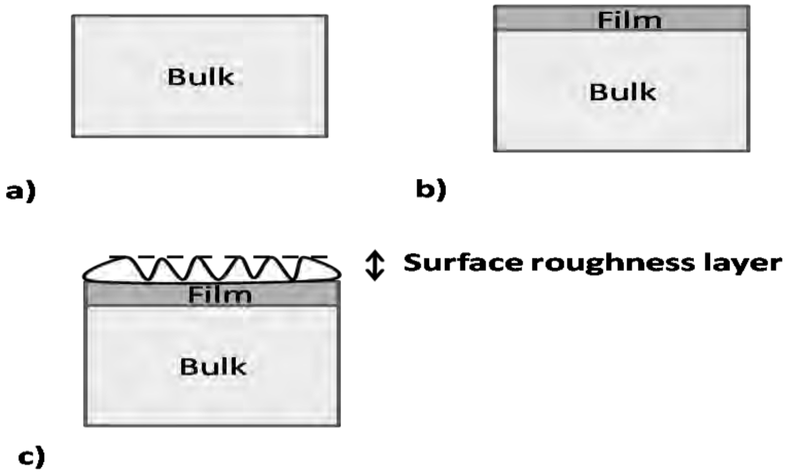

Figure 4.9 – Various optical models for spectroscopy ellipsometry.

We used models in Figure 4.9a and b in our analysis of data. But constructing those models, we are making an assumption that the samples are flat and smooth. But these are ideal scenarios. For the case of graphene on SiO2/Si. a surface roughness layer should be added as it has been shown experimentally from other literatures [31-34] that a thin roughness layer (corrugations) forms on graphene surface. These corrugations are intrinsic as well as substrate induced [35-36]. The addition of roughness layer to our optical model remains to be future work to be carried out. Meanwhile, it has to be emphasized that although the fitting of Si and SiO2 turns out to be acceptable, the optical models constructed is only a rough estimation to the real structure of the sample and thus independent estimation of the sample structure has to be carried out with other experimental techniques like atomic force microscopy (AFM) or transmission electron microscope (TEM). Working hand in hand with these experimental techniques can give us information to better construct the optical model and get a better fitting.

Secondly, it remains to be an open question whether the addition of a surface roughness layer on the optical model of graphene on SiO2/Si would differ our current experimental optical conductivity spectrum. If there is no difference, then the blue shift and lesser degree of asymmetry compared to the theoretical spectrum of free standing graphene is clearly due to substrate interaction. The e-h interaction, as mentioned in Section 1.2 causes a redistribution of the oscillator strength, causing the energy peak of the optical conductivity of free standing graphene to drop from 5.2eV (GW calculations) to 4.6eV (GW-BSE calculation). The e-h interaction also causes an asymmetry to the optical conductivity of free-standing graphene. These implies that there could be a screening of e-h interactions in graphene on SiO2/Si, which causes the blue shift as well as the lesser degree of asymmetry. These screenings could be due to substrate induced charge impurities but with regards to the extent they screen the e-h interactions, more studies need to be conducted.

4.5 SUMMARY

In this chapter, we have looked at our experimental results. Both the dielectric functions of c-Si and SiO2 turns out to be in agreement with other literatures. We also gave a rough estimation to the acceptable MSE value, and using this guideline, we found that fitting graphene on SiO2/Si is unreasonable. The experimental optical conductivity of graphene on SiO2/Si, when compared with the theoretical calculation of free-standing graphene, shows a blue-shift and a lesser degree of asymmetry. Before we quickly associate those observations to graphene-substrate interaction, we have to construct a more accurate representation of the optical model that includes the corrugations and extract a new optical conductivity spectrum. If the new optical conductivity spectrum still resembles our current spectrum, we can conclude that there is an interaction between graphene and SiO2 substrates such that it leads to a screening of e-h interaction.

CHAPTER 5 SUMMARY AND FUTURE DIRECTIONS

5.1 SUMMARY

In our thesis, we want to study the resonant excitonic effects of graphene on SiO2/Si, using spectroscopic ellipsometry. We compared this experimental technique with reflectance spectroscopy in Chapter 2, and we found out through our simulation that the data analysis of a single layered sample is more accurate than that of reflectance spectroscopy as the latter requires the use of Kramers-Kronig relations which requires an extrapolation of data. We also justified that spectroscopy ellipsometry is suitable for our experiment as the quantities measured are very sensitive to ultrathin layers. Through curve fitting, we are able to extract the optical spectra of multilayered samples and calculate the MSE values. Our experimental results were presented in Chapter 4. The experimental optical conductivity of graphene on SiO2/Si, when compared with the theoretical calculation of free-standing graphene, shows a blue shift (4.0eV to 4.65eV) and a lesser degree of asymmetry. However, before we quickly associate those observations to graphene-substrate interaction, we have to construct a more accurate representation of the optical model that includes the corrugations. The curve fitting of graphene on SiO2/Si for 70^0 incidence angle shows very high MSE at 0.289^0 and there is a high chance that the optical model constructed was wrong. Meanwhile, if the new optical conductivity spectrum still resembles our current experimental spectrum, we can conclude that there is an interaction between graphene and SiO2 substrates such that it leads to a screening of e-h interaction.

5.2 FUTURE DIRECTIONS

It requires further work to understand the resonant excitonic effects in graphene on SiO2/Si. Firstly, the optical model has to include the roughness layer, which involves a different mathematical formulation. Also, to ensure that our optical models are constructed accurately, it is required that for the samples to be studied under other optical measurements like AFM or STM.

REFERENCES

[1] Geim, A. K. & Novoselov, K. S. The rise of graphene. Nature Matter. 6, 183–191, 2007.

[2] J. W. Weber, V. E. Calado, and M. C. M. van de Sanden. Optical constants of graphene measured by spectroscopic ellipsometry. Applied Physics Letters 97, 091904, 2010.

[3] H. Fujiwara, Spectroscopic ellipsometry principles and applications, John Wiley & Sons, West Sussex, 2007.

[4] H. G. Tompkins and W. A. McGahan, Spectroscopic Ellipsometry and Reflectometry, A User‟s Guide,Wiley, New York,1999

[5] Mark Fox. Optical Properties of Solids. Oxford Master Series,2010.

[6] J.A Woollam Co. Inc. Dielectric Function. Retrieved from: http://www.jawoollam.com/dielectric_function.html on 1st April 2014.

[7] L.Mihaly, Kramers-Kronig relations, Budapest University of Technology and Economics, 2006.

[8] A. B. Kuzmenko, Kramers–Kronig Constrained Variational Analysis Of Optical Spectra, Rev. Sci. Instrum. 76, 083108, 2005.

[9] Ariando. PC3251, Nanophysics Lecture 8: Two Dimensional Electron System in a Quantum Well. National University of Singapore,2013.

[10] U. Schmid, N. E. Christensen, and M. Cardona. Relativistic band structure of Si, Ge, and GeSi: Inversion-asymmetry effects. Physical Review B, Volume 41, Number 9,1990.

[11] Iman Santoso et.al. Tunable optical absorption and interactions in graphene via oxygen plasma. Phys. Rev. B 89, 075134, 2014.

[12] D. E. Aspnes. Optical-standard surfaces of single-crystal silicon for calibrating ellipsometers and reflectometers . Applied Optics, Vol. 33, Issue 31, pp. 7435-7438, 1994

[13] D. E. Aspnes . Optical Properties of thin solid films. Thin Solid Film, 89, 249-262, 1982.

[14] R.B Laughlin. Optical Absorption edge of SiO2. Phys. Rev. B22, 3021, 1980.

[15] A. H. Castro Neto et.al. The Electronic Properties of Graphene. Reviews Of Modern Physics.Vol. 81,2009 .

[16] Phaedon Avouris. Graphene: Electronic and Photonic Properties and Devices. Nano Lett., 2010, 10, 2011.

[17] Li Yang et.al. Excitonic Effects on the Optical Response of Graphene and Bilayer Graphene. PRL 103, 186802, 2009.

[18] Xu Du et.al. Approaching Ballistic Transport In Suspended Graphene. Nature Nanotechnology. Vol.3, 2008.

[19] Jason Horng et.al. Drude Conductivity of Dirac Fermions in Graphene. Phy.Rev B 83,165113, 2011.

[20] N.M.R.Peres. The Transport Properties of Graphene: An Introduction. Rev.Mod.Phys.82:2673-2700,2010.

[21] K.F. Mak et.al. Optical spectroscopy of graphene: From the far infrared to the ultraviolet . Solid State Communications 152 , 2012.

[22] K.F. Mak et.al. Seeing Many Body Effects in Single-and Few Layers Graphene: Observation of Two-Dimensional Saddle Point Excitons. PRL. 106, 046401, 2011.

[23] U.Fano. Effects of Configuration Interaction on Intensities and Phase Shifts. Phys.Rev. Vol.124 No.6, 1961.

[24] J.C. Yong, W. Chegal and M.C. Hyun. Fourier Analysis For Rotating-Element Ellipsometer. Optics Letters, Vol.36, No.2, 2011.

[25] Michael B. Wallace, Adam Wax, David N. Roberts, Robert N. Graf. Reflectance Spectroscopy. Gastrointestinal Endoscopy Clinics of North America, Volume 19, Issue 2, Pages 233-242.

[26] H. R. Philipp And E. A. Taft. Optical Constants Of Germanium In The Region I To 10 Ev. P Hys I Cal Review. Volume 1&3, Number 41959.

[27] S. S. Ng, Z. Hassan & H. Abu Hassan. Kramers-Kronig Analysis Of Infrared Reflectance Spectra With A Single Resonance. Universiti Teknologi Malaysia. Jurnal Teknologi, 44(C) : 67–76, Jun 2006.

[28] D. M. Roessler. Kramers - Kronig Analysis Of Non-Normal Incidence Reflection. Brit. J. Appl. Phys. Vol. 16, 1965

[29] Horiba Scientific. Spectroscopy Ellipsometry. Retrieved from: http://www.horiba.com/scientific/products/ellipsometers/ellipsometryacademy/faqs/basic/ on 19Feb 2014.

[30] G.E.Jellison,Jr. Use Of The Biased Estimator In The Interpretation Of Spectroscopy Ellipsometry Data. Applied Optics, Vol. 30, Issue 23, Pp. 3354-3360, 1991.

[31] SPIE. Growing better graphene by finding the best copper substrate. Adapted from https://spie.org/x85353.xml on 4th April 2014.

[32] Joshua D. Wood. et.al. Effects of Polycrystalline Cu Substrate on Graphene Growth by Chemical Vapor Deposition. Nano Lett. pp 4547–4554, 2011.

[33] Yi Zhang Et.Al Review Of Chemical Vapor Deposition Of Graphene And Related Applications. Accounts of Chemical Research. 2329-2339.Vol.46.No.10, 2013.

[34] Matthew O"Brien.et.al. CVD Synthesis and Characterization of Graphene Thin Films. Army Research Laboratory, 2010.

[35] Masa Ishigami. et.al. Atomic Structure of Graphene on SiO2. Nano Letters. Vol. 7, No. 6, 1643-1648, 2007.

[36] J. C. Meyer. et.al. On the roughness of single- and bi-layer graphene membranes. Solid State Communications. Volume 143. Issues 1–2,.Pages 101–109, 2007.